Understanding the Role of Macrophages in Lung Inflammation Through Mathematical Modeling

Sarah B. Minucci[a], Rebecca L. Heise[b,c], Michael S. Valentine[b], Franck J. Kamga Gninzeko[b], Angela M. Reynolds[a,c,*]

[a] *Virginia Commonwealth University, Department of Mathematics & Applied Mathematics, 1015 Floyd Avenue, Box 842014, Richmond, VA 23284*

[b] *Virginia Commonwealth University, Department of Biomedical Engineering, 601 West Main Street, Box 843068, Richmond, Virginia 23284*

[c] *Victoria Johnson Center, Virginia Commonwealth University, Richmond, Virginia 23284*

Abstract

Respiratory infections, such as the novel coronavirus (SARS-COV-2), and other lung injuries infect and damage the pulmonary epithelium. In the most severe cases this leads to acute respiratory distress syndrome (ARDS). Due to respiratory failure associated with ARDS, the clinical intervention is the use of mechanical ventilation. Despite the benefits of mechanical ventilators, pro-longed or misuse of these ventilators may lead to ventilation-induced lung injury (VILI). Damage caused to epithelial cells within the alveoli can lead to various types of complications and increased mortality rates. A key component of the immune response is recruitment of macrophages, immune cells that differentiate into phenotypes with unique pro- and/or anti-inflammatory roles based on the surrounding environment. An imbalance in pro- and anti-inflammatory responses can have deleterious effects on the individual's health. To gain a greater understanding of the mechanisms of the immune response to VILI and post-ventilation outcomes, we develop a mathematical model of interactions between the immune system and site of damage while accounting for macrophage polarization. Through Latin Hypercube Sampling and available data, we generate a virtual cohort of patients with biologically feasible dynamics. We use a variety of methods to analyze the results, including a random forest decision tree algorithm and parameter sensitivity with eFAST. Analysis shows that parame-

*Corresponding author

Email addresses: minuccisb@vcu.edu (Sarah B. Minucci), rlheise@vcu.edu (Rebecca L. Heise), msvalentine@vcu.edu (Michael S. Valentine), kamgagninzefj@vcu.edu (Franck J. Kamga Gninzeko), areynolds2@vcu.edu (Angela M. Reynolds)

ters and properties of transients related to epithelial repair and M1 activation and de-activation best predicted outcome. Using this new information, we hypothesize interventions and use these treatment strategies to modulate damage in select virtual patients.

Keywords:
Mechanical Ventilation, Lung Inflammation, Mathematical Modeling, Epithelial Cells, Macrophage Polarization

---

1. Introduction

Inflammation occurs in the lungs when an immune response is initiated to eliminate an insult. Types of insults include inhaled pathogens, such pneumonia, tuberculosis or COVID-19, or harmful particles. In the most severe cases this leads to acute respiratory distress syndrome (ARDS). Due to respiratory failure associated with ARDS, the clinical intervention is the use of mechanical ventilation. When COVID-19 infected individuals symptoms become severe, it can lead to respiratory failure and death of the patients. In recent study, two thirds patients admitted for COVID-19 required mechanical ventilation (Mahase, 2020).

Despite the benefits of mechanical ventilators, pro-longed or misuse of these ventilators may lead to ventilation-induced lung injury (VILI). In this work we will focus on the tissue damage associated with mechanical ventilation and resulting immune cell recruitment. The damage caused to alveolar sacs (clusters of alveolar cells) during mechanical ventilation can lead to volutrauma (extreme stress/strain), barotrauma (air leaks), atelectrauma (repeated opening and closing of alveoli), and biotrauma (general severe inflammatory response). If the trauma increases, it can lead to multi-system organ failure (Halbertsma et al., 2005; Slutsky and Ranieri, 2013). It has also been shown that the inflammatory response of the elderly is altered in the lungs and other areas (Provinciali et al., 2011; De Rekeneire et al., 2006). As compared to younger individuals, increased levels of circulating inflammatory cytokines and different immune cell function has been reported in older patients (Canan et al., 2014). A 2003-2008 study conducted at Bridgeport Hospital reported that 4,238 out of 9,912 (42.8%) patients received mechanical ventilation for a median of two days. Mortality or discharge to extended-care facilities increased for each decade of age greater than 65 years (Feng et al., 2009). Additionally, the case fatality rate for COVID-19 patients over 70-year-old and over 80-year-old was around 50.8% and 14.8% of the total number of deaths, respectively (Wu and McGoogan, 2020). This is in agreement with other studies reporting higher rates of severe outcomes in patients with COVID-19 aged 65 or more (Bruno et al., 2020). The increase in the

severity of VILI with patient age combined with the increased need for ventilation and increased mortality rate among the elderly stresses the need to investigate the influence of aging in VILI. The framework we have built here addresses VILI with various parameters and initial conditions that can be narrowed, in future studies, with data from different age groups and insults to explore dynamics and driving factors in diseases.

Through mathematical modeling, we can understand more about the pulmonary immune response and how treatments can be most effective in combating damage to alveoli and immune cells. Towards this goal, we adapted a model developed by Torres et al. for the innate immune response to bacteria, which accounts for macrophage polarization, to include epithelial dynamics and stretch-induced recruitment of immune cells (Torres et al., 2019). We use this model to understand the mechanisms by which the immune system responds to damaged epithelial cells and the sensitivity of post-ventilation outcome to components of this complex process. We begin this study by analyzing the epithelial subsystem mathematically. This allows us to understand fixed point stability and how various parameters affect stability for the new portion of the model. The full model is a large system of ordinary differential equations with a large number of parameters and a variety of nonlinear dynamics. Allowing the parameters in the model to vary over biologically feasible ranges using Latin Hypercube sampling simulates the variety of immune system dynamics observed in patients. We organize disease progressions into three categories, healthy, persistent inflammation, and dying, based on the percentage of epithelial cells that are healthy. To determine what is driving differences in outcome, we use a variety of methods to analyze the resulting dynamics: 1) comparison of parameters associated with different outcomes, 2) random forest decision tree algorithm, which parses through the variety of predictors that may be particularly important in the immune response to VILI and 3) parameter sensitivity with eFAST, a variance-based method.

1.1. Biological background

The alveolar epithelium consist of alveolar type I and type II cells. Alveolar type I cells make up about 95% of the alveolar surface and are primarily responsible for facilitating gas exchange. Type II cells cover the other 5% of the surface and are important in the innate immune response. In the presence of damage, these cells proliferate to repair the epithelium and can also differentiate to type I cells (Matthay et al., 2005; Mason, 2006). The extent to which the alveolar epithelium is damaged is a useful indicator of the overall effects of a lung insult (Ware and Matthay, 2000).

The immune response is divided into innate (non-specific) and adaptive (acquired) responses. Two of the most important innate immune cells are neutrophils and

macrophages, which can be tissue-specific or recruited to the site upon damage. This response is always present and ready to defend against pathogens or other insults. On the other hand, the adaptive immune response includes B and T cells, which differentiate in such a way that they are effective at fighting specific pathogens. They are recruited by antigen-presenting cells, such as dendritic cells and macrophages, that are a part of the innate immune response. We concentrate on the innate immune system when modeling VILI to gain a better understanding of the epithelial and immune cell interactions. Lung infection may lead to the need for mechanical ventilation and the resulting model could be adapted to study mechanical ventilation with infection in the future. Initially we consider a system in which the immune response is triggered by damage associated with the ventilator without infection.

One of the key components of this response is recruitment of macrophages from the bone marrow and bloodstream to the damaged area to support the population of resident alveolar macrophages. Macrophages send signals to other immune cells and aid in the process of eliminating dead cells and repairing damaged ones Aggarwal et al. (2014). Phenotypes of macrophages can range from "pro-inflammatory" (M1) or "anti-inflammatory" (M2) based on their activators and byproducts (Mosser and Edwards, 2008; Wang et al., 2014). Their pro-inflammatory behavior includes destroying the pathogen, consuming damaged cells, and amplification of signaling. Their anti-inflammatory response, which counteracts pro-inflammatory behavior, promotes repair by producing anti-inflammatory cytokines and removing apoptotic neutrophils. A single macrophage may produce both pro-inflammatory and anti-inflammatory signals concurrently, which can make classification and identification of phenotype a difficult question.

Another important type of immune cell is neutrophils, which respond quickly to pro-inflammatory signals sent from damaged epithelial cells and other resident cells. A small amount of neutrophils are found in the lungs in homeostasis; however, neutrophils are recruited from bone marrow in response to pro-inflammatory signals from damaged epithelial cells and resident macrophages during an insult in large numbers (Kolaczkowska and Kubes, 2013). Neutrophils have phagocytic capabilities in the presence of invading pathogens, but in the case of VILI without infection neutrophils recruit other immune cells such as macrophages through the production of pro-inflammatory agents such as proteinases and cytokines and contribute to the removal of damaged or dead tissue. An overabundance of neutrophils and their byproducts can cause further unnecessary damage (Grommes and Soehnlein, 2011). Neutrophils are relatively short-lived; they become apoptotic and are removed by macrophages (Kolaczkowska and Kubes, 2013) or become necrotic in an uncontrolled death resulting in the release of cytotoxic material (Naylor et al., 2007).

An imbalance in the pro- and anti-inflammatory responses can cause complications for the individual. Furthermore, an absence of immune cells can lead to immunodeficiency and a surplus of immune cells can result in chronic inflammation (Kolaczkowska and Kubes, 2013). Thus, it is important to understand the immune response to lung injury and the interplay between various types of cells. It is also believed that macrophages play a significant role in the impact of immune response on aging (Canan et al., 2014; Linehan and Fitzgerald, 2015; Mahbub et al., 2011).

1.2. Mathematical background

Mathematical modeling is used to capture the complexities of the immune response to epithelial cell damage, including important feedback loops and nonlinearities. Analyzing the resulting model gives insight into the driving mechanism of this system. An *in silico* approach allows us to simulate various scenarios or new treatments, especially when *in vivo* and *in vitro* experiments to explore possible intervention to improve outcome for patients are difficult to perform. To our knowledge, no mathematical models have described M1/M2 interactions specific to the immune response to VILI. Many models have examine the immune response to bacterial and viral infections, such as pneumonia (Schirm et al., 2016; Mochan et al., 2014; Smith et al., 2011), tuberculosis (Day et al., 2009; Raman et al., 2010; Segovia-Juarez et al., 2004), and influenza (Manchanda et al., 2014; Anderson et al., 2016; Hancioglu et al., 2007). Additionally, models related to smoking and asthma (Brown et al., 2011; Chernyavsky et al., 2014; Golov et al., 2017; Pothen et al., 2015), mechanical ventilation (Hickling, 1998; Marini et al., 1989; Pidaparti et al., 2013), and general inflammatory stress (Reynolds et al., 2010) have been developed, but these models generally deal with the mechanics of the airways, including airflow, pressure, and gas exchange, and how these mechanics respond to inflammation and particle inhalation without accounting for the various cells types involved in the immune response. Models have also been developed to understand and analyze the molecular mechanisms that govern the phenotype switch that macrophages undergo from pro-inflammatory to anti-inflammatory, as well as other important subcellular pathways (Anderson et al., 2016; Braun et al., 2013; Maiti et al., 2014).

Common modeling approaches used in these papers include agent based modeling (Brown et al., 2011; Pothen et al., 2015; Segovia-Juarez et al., 2004), partial differential equations (Pidaparti et al., 2013; Reynolds et al., 2010), ordinary differential equations (Chernyavsky et al., 2014; Day et al., 2009; Hancioglu et al., 2007; Mochan et al., 2014; Schirm et al., 2016; Smith et al., 2011), and Boolean models (Anderson et al., 2016). Each technique has its advantages and disadvantages, but we choose to model the inflammatory response to VILI, specifically the resulting damage to

epithelial cells, using a set of coupled ordinary differential equations (ODEs), which we describe further in the following section. Systems of ODEs are ideal for modeling dynamical systems because of their ability to capture, with reasonable computation times, the highly nonlinear behavior of the many immune cells, epithelial cells and other mediators involved in the immune response to VILI. This allows for mathematical and sampling approaches to be used in order to determine key components of the model.

2. Methods & Model Development

2.1. Experimental materials & methods

Animals: Male C57BL/6 mice 8 weeks of age were purchased from Jackson Laboratory (Bar Harbor, ME). Male C57BL/6 mice 20 months of age were provided by the National Institute on Aging (Bethesda, MD). All animals were housed in accordance with guidelines from the American Association for Laboratory Animal Care and Research protocols and approved by the Institutional Animal Care Use Committee at Virginia Commonwealth University (Protocol No. AD10000465).

Pressure-Controlled Ventilator-Induced Lung Injury Model: We mechanically ventilated young (2-3 mo) and old (20-25 mo) C57BL/6J wild-type mice using a Scireq FlexiVent computer-driven small-animal ventilator (Montreal, Canada) and previously cited methods (Herbert et al., 2016) with slight modifications. Mice were anesthetized, tracheotomized, and then ventilated for 5 minutes using a low pressure-controlled strategy (peak inspiratory pressure (PIP): 15 cmH20, respiratory rate (RR): 125 breaths/min, positive end-expiratory pressure (PEEP): 3 cmH20). Mice were then ventilated for 2 hours using a high pressure-controlled mechanical ventilation (PCMV) protocol (PIP: 35-45 cmH20, RR: 90 breaths/min, and PEEP: 0 cmH20). Pulmonary function and tissue mechanics were measured and collected at baseline and every hour during the 2-hour high PCMV duration using the SCIREQ FlexiVent system and FlexiWare 7 Software. A separate group of mice was anesthetized, tracheotomized, and maintained on spontaneous ventilation for 2 hours.

Tissue Processing: Immediately following mechanical ventilation, the right lobes of the lung were snap frozen with liquid nitrogen, then stored at -80°C for further analysis. The left lobes of the lung were then inflated with digestion solution containing 1.5 mg/mL of Collagenase A (Roche) and 0.4 mg/mL DNaseI (Roche) in HBSS with 5% fetal bovine serum and 10mM HEPES and processed as previously described (Yu et al., 2016). The resulting cells were counted, and dead cells were excluded using trypan blue. Subsets of the experimental groups were also used to collect bronchoalveolar lavage fluid (BALF) fluid, differential cell counts, and left lobes for histological analysis.

Flow Cytometric Analysis: Following live cell counts, 4×10^6 cells per sample were incubated in blocking solution containing 5% fetal bovine serum and 2% FcBlock (BD Biosciences) in PBS. The cells were then stained using a previously validated immunophenotyping panel of fluorochrome-conjugated antibodies (Misharin et al., 2013) with slight modifications (See Table S1 in Supplementary Material for a list of antibodies, clones, manufacturers, and concentrations). Following the staining procedure, cells were washed and fixed with 1% paraformaldehyde in PBS. Data were acquired and analyzed with a BD LSRFortessa-X20 flow cytometer using BD FACS-Diva software (BD Bioscience). Histogram plots were generated using FCS Express 5 software (De Novo). Compensation was performed on the BD LSRFortessa-X20 flow cytometer at the beginning of each experiment. "Fluorescence minus one" controls were used when necessary. Cell populations were identified using a sequential gating strategy that was previously developed (Misharin et al., 2013). The expression of activation markers was presented as median fluorescence intensity (MFI).

Statistics: A total of 10 young mice were used for this study. Data is shown for each type of activation (M0, M1, M2) as a percentage of the total macrophages.

2.2. Epithelial subsystem

The primary focus of this model is to examine the effects of damage on the alveolar epithelium, in particular alveolar type II cells since they are responsible for restoration of the epithelium. In this section we begin with a simple model, concentrating on the novel aspect of incorporating epithelial cells and relative damage due to inflammation, then add variables to more accurately model the dynamics within this system.

We begin with a small three-dimensional system of differential equations, shown in Equations (1)-(3), where E_h is the proportion of the local space filled by healthy cells, E_d is the proportion of the local space filled by damaged cells, and E_e represents dead cells awaiting removal by phagocytic immune cells or empty "space" to be filled with new, healthy cells. Each term represents a biological event explained by the brackets above the term. This first model includes only the baseline abilities of epithelial cells to proliferate and repair themselves in the presence of sustained damage. We do not explicitly model proliferating and non-proliferating cells; the parameter p is modulated to reflect the general mechanism by which neighboring epithelial cells renew exposed areas.

$$\frac{dE_h}{dt} = \overbrace{p(E_h + E_d)(E_e)}^{\text{Proliferation}} + \overbrace{rE_d}^{\text{Repair}} - \overbrace{sE_h}^{\text{Damage}} \tag{1}$$

$$\frac{dE_d}{dt} = -\overbrace{rE_d}^{\text{Repair}} - \overbrace{bE_d}^{\text{Death}} + \overbrace{sE_h}^{\text{Damage}} \tag{2}$$

$$\frac{dE_e}{dt} = \overbrace{p(E_h + E_d)(E_e)}^{\text{Proliferation}} + \overbrace{bE_d}^{\text{Death}} \tag{3}$$

Damage from stretch due to mechanical ventilation is represented by the rate s, and causes healthy epithelial cells to become damaged. Some damaged cells, depending on the severity of damage, have the ability to repair themselves, returning from the E_d state back to E_h, represented by a baseline repair rate r (Crosby and Waters, 2010). Damaged cells may also decay naturally at a rate b.

The first term in the equations representing healthy cells, Equation (1), and empty cells, Equation (3), accounts for proliferation of the healthy and damaged cells into empty space. Nearby epithelial cells and progenitor cells, stem cells that can differentiate into specific types of epithelial cells only, perform this task. These cells spread and replicate to fill the empty space left by dead epithelial cells (Crosby and Waters, 2010; Gardner et al., 2010; Herold et al., 2011). In this model we account for proliferation associated with local epithelial cells. Multiplying by E_e in this term scales the proliferation rate such that the term is increased (less contact inhibition) when there is more empty space. Note that total local space is conserved: $E_e + E_h + E_d = 1$. Therefore, we can define $E_e = 1 - (E_h + E_d)$ and rewrite this term as logistic growth with a carrying capacity of 1. This gives rise to a two dimensional system, Equations (4)-(5).

$$\frac{dE_h}{dt} = \overbrace{p(E_h + E_d)(1 - (E_h + E_d))}^{\text{Proliferation}} + \overbrace{rE_d}^{\text{Repair}} - \overbrace{sE_h}^{\text{Damage}} \tag{4}$$

$$\frac{dE_d}{dt} = -\overbrace{rE_d}^{\text{Repair}} - \overbrace{bE_d}^{\text{Death}} + \overbrace{sE_h}^{\text{Damage}} \tag{5}$$

Stability analysis reveals that in the absence of stretch ($s = 0$) and with all positive parameters, $(0, 0)$ is a saddle node and $(0, 1)$ is a stable equilibrium with eigenvalues $\lambda_1 = -r - b$ and $\lambda_2 = -p$. Given a nonzero initial condition for damaged cells the epithelial cells subsystem will resolve to the fully repaired fixed point $(0, 1)$.

In the presence of sustained stretch ($s > 0$), the E_d nullcline switches from a vertical line to a line with slope $(r + b)/s$. The second equilibrium point changes from (0,1) to

$$(E_d^*, E_h^*) = \left(\frac{s^2(p-b) + ps(b+r)}{p(b^2 + r^2 + s^2 + 2br + 2bs + 2rs)}, \frac{(r+b)[s(p-b) + p(b+r)]}{p(b^2 + r^2 + s^2 + 2br + 2bs + 2rs)} \right)$$

Therefore in the presence of damage, there no longer exists an equilibrium associated with full recovery.

Exploratory simulations demonstrate that there is a bifurcation with respect to p, proliferation rate of the epithelial cells. A bifurcation diagram for this parameter, shown in Figure 1, has one transcritical bifurcation at $p^* = 0.497$. In this figure, we show the proportion of space occupied by healthy epithelial cells as a percentage, which is E_h multiplied by 100. The second equilibrium for p values below the bifurcation is not included in the diagram, since it is non-biological (negative E_h). For small values of p, the ability of healthy cells to proliferate and replace dead cells is insufficient and damage causes both healthy and damaged cells to approach 0%. On the other hand, for values of p larger than p^*, the system approaches the stable nonzero equilibrium (E_d^*, E_h^*), which is closer to (0,1) for higher values of p even in the presence of sustained damage.

2.3. Fixed immune response

Next we examine the roles of immune cells, especially neutrophils and macrophages, by adding several terms to Equations (1) and (2). We first focused on dynamics with a fixed immune response, because when we work with the full model (described in the next section), we only consider parameter sets that give rise to steady state solutions in the absence of damage. Therefore, we decided to start our model development by analyzing E_h and E_d with immune cells as parameters before including their dynamics. The modifications are shown in Equations (6) and (7).

$$\frac{dE_h}{dt} = \overbrace{p(E_h + E_d)(1 - (E_h + E_d))}^{\text{Proliferation}} + \overbrace{rE_d}^{\text{Repair}} - \overbrace{sE_h}^{\text{Damage}} - \overbrace{nE_h}^{\text{Collateral damage from neutrophils}} \tag{6}$$

$$\frac{dE_d}{dt} = -\overbrace{rE_d}^{\text{Repair}} - \overbrace{bE_d}^{\text{Death}} + \overbrace{sE_h}^{\text{Damage}} + \overbrace{nE_h}^{\text{Collateral damage from neutrophils}} - \overbrace{mE_d}^{\text{Removal of damaged cells by macrophages}} \tag{7}$$

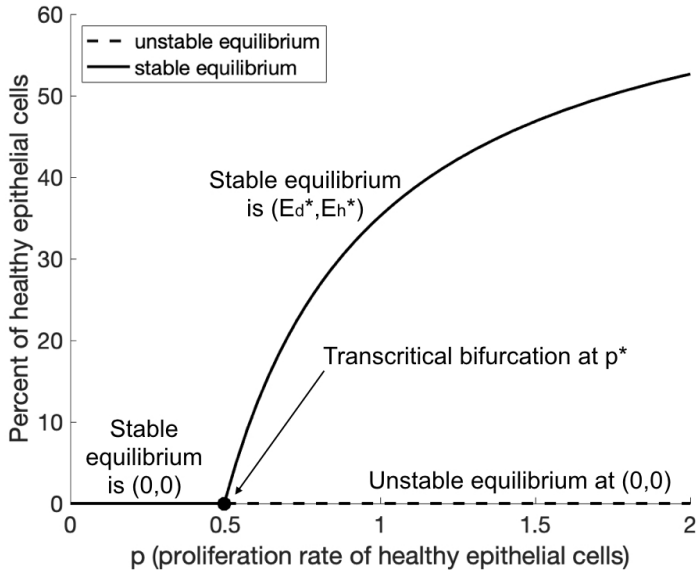

Figure 1: Bifurcation diagram for the proliferation parameter p for the epithelial system with stretch and no immune response. Other parameters are set to $r = 2.6$, $s = 0.22$, and $b = 0.74$. The unstable equilibrium below $p < p^* = 0.497$ is not included in the figure, since it is not biologically relevant.

The physical presence of immune cells, especially first-responder neutrophils, cause small-scale collateral damage as they clear debris (Nathan, 2006) and can be especially deleterious if the response is overzealous (Grommes and Soehnlein, 2011). This biological event is modeled as the last term in Equation (6) with cells switching from a healthy to a damaged state at the rate n. M1 macrophages aid in the clearance of damaged cells to make room for replacement by new, healthy cells through subcellular signalling and phagocytosis (Aggarwal et al., 2014; Gardner et al., 2010). The last term in Equation (7) represents this loss of damaged cells.

The stability analysis is similar to that from the model without the immune response, with additional parameters m, n that can shift steepness of the nullcline or the speed at which the system approaches or diverges from an equilibrium. The parameter p once again plays an important role in the stability of the two critical points, $(0, 0)$ and

$$(E_d^*, E_h^*) = \left(\frac{(n+s)[(n+s)(p-b-m)+p(b+m+n)]}{p(b+m+n+r+s)^2}, \frac{(b+m+r)[(n+s)(p-b-m)+p(b+m+n)]}{p(b+m+n+r+s)^2} \right)$$

The equilibria result in a transcritical bifurcation for changing values of p similar to Figure 1. The main difference is that the transcritical bifurcation point p^* is lower because of the damage resulting from macrophages and neutrophils, represented by m and n. The rate of proliferation of healthy cells must be higher to counteract these effects.

The bifurcation diagram for scaled E_h versus n also has a transcritical bifurcation (see Figure 2a). For sufficiently low values of n, the nonzero critical point is stable, but for values above $n^* = 1.364$, $(0, 0)$ is the stable equilibrium. Additionally, the two-parameter stability diagram shows a curve which separates the p/n-space into two stability regimes (see Figure 2b). For high enough values of n and low enough values of p, the system goes to zero for both variables. Biologically, this corresponds to a situation in which the ability of epithelial cells to proliferate is low and there are high levels of immune cells. On the other hand, with low levels of immune cells and a higher proliferation rate, the system limits to the nonzero equilibrium. It should be noted that for a large enough p, it would take an extremely high value of n to overpower proliferation and make $(0, 0)$ the stable critical point. In the full system the initial conditions for our simulations will have similar properties to the type of steady state in the non-zero stable equilibrium region of Figure 2b.

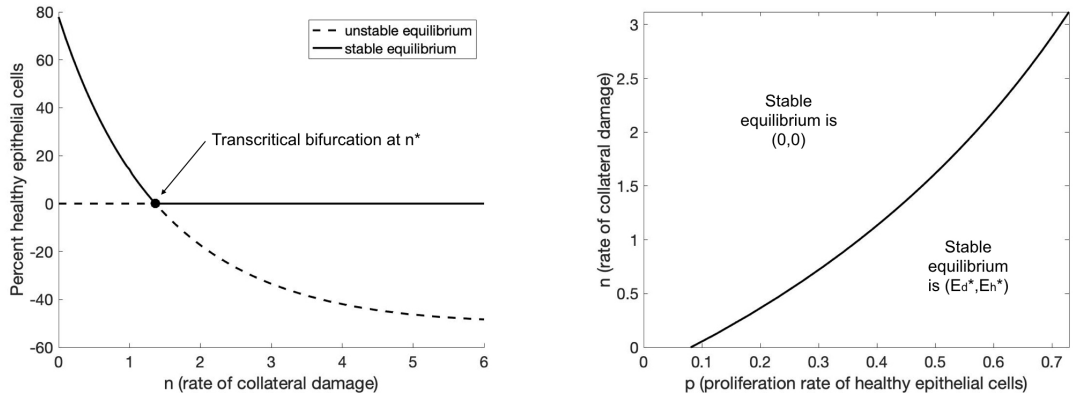

(a) (b)

Figure 2: (a) Bifurcation diagram for epithelial subsystem when varying n. Other parameter values are set to $r = 2.6$, $p = 0.45$, $s = 0.22$, $b = 0.74$, $n = 1.6$, $m = 0.92$. (b) Two-parameter plot showing values of p and n which cause the subsystem to have either a zero or nonzero stable equilibrium.

These simple models provide a framework for the dynamics of the epithelium in response to damage and an introductory look into the influence of the immune response. However, there are many more complex, nonlinear interactions and events involved in VILI which we will explore in the next section.

2.4. Development of complete model

By adding variables to the two-dimensional system proposed above, we develop a system of coupled ordinary differential equations to model the interactions between immune cells, epithelial cells, and other mediators shown in Figure 3. We also utilize a two-compartment method in which resident immune cells respond to the damaged epithelial cells and nonresident immune cells are recruited from the bloodstream.

A system of ODEs is ideal for modeling these interactions because of its ability to capture distinct nonlinearities and feedback loops with relatively low computational requirements. However, one of the drawbacks of an ODE model is that it assumes a well-mixed environment, in which all elements of the model are evenly distributed throughout the given space. Biologically, this is not always the case. One way to to include aspects of the spatial heterogeneity without explicitly modeling space is to use a compartmental model. Each compartment represents a well mixed environment and, when biologically appropriate, variables can move between compartments. An ODE can represent an immune system component in each compartment in which it may exist.

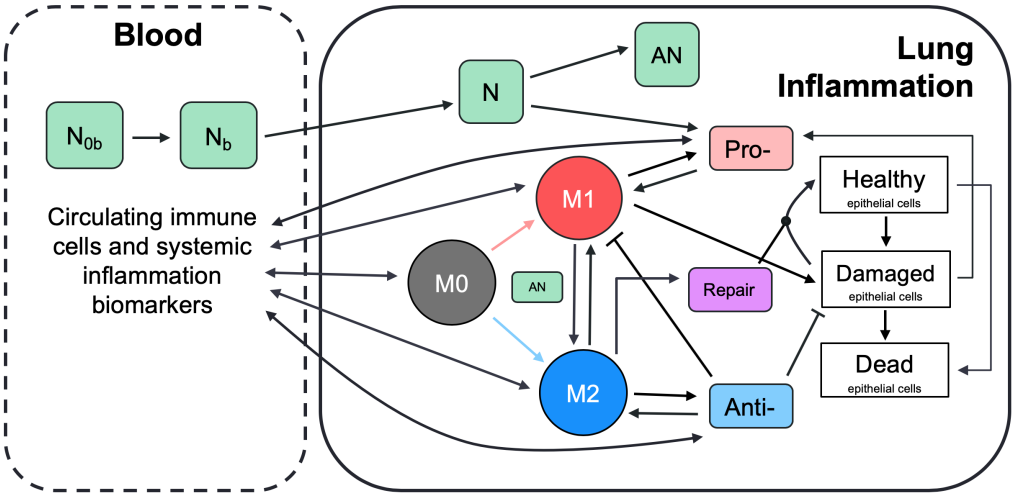

Figure 3: Schematic describing interactions between macrophages, neutrophils, various pro- and anti-inflammatory mediators, and epithelial cells. Red boxes represent various types of neutrophils, colored circles represent M0, M1, and M2 macrophages, green boxes represent various types of factors and mediators that act as signals to immune cells, and white boxes represent healthy, damaged, and dead epithelial cells. Damaged epithelial cells (E_d) release pro-inflammatory mediators (p_b & p) which recruit resting macrophages (M_0) and free-flowing neutrophils (N_{0b}) from the bloodstream. Unactivated immune cells become activated by various cytokines, factors, and proteins and perform either pro-inflammatory or anti-inflammatory roles which are meant to remove debris (E_e) and promote repair of damaged epithelial cells.

Here we choose to model two compartments. The first is the site of inflammation in the lungs, specifically the epithelial cells which provide a barrier lining the alveolar cells. The second compartment is the adjacent blood vessel that provides additional immune support to the site of damage. Differentiating between these two compartments allows us to determine the concentrations of various immune cells and other mediators in each separate area and examine their movement across compartments. A two-compartmental model accounts for some spatial dynamics that a traditional system of ODEs cannot, making the model more realistic for a better understanding of the immune response to VILI.

Figure 3 gives a detailed breakdown of the dynamics in the lung. The dynamics are similar for those cells and mediators that are in the blood. Cell types that are tracked in each compartment are stated in Table 1. In the following subsections, we develop the equations for these variables. The parameters used in used in the equations are given in Table 2 with their description and range used during parameter sampling.

Bloodstream	Lung	Description
	E_h	Healthy epithelial cells
	E_d	Damaged epithelial cells
	E_e	Dead epithelial cells/empty space
p_b	p	Pro-inflammatory mediators
a_b	a	Anti-inflammatory mediators
M_{0b}	M_0	Unactivated macrophages
M_{1b}	M_1	M1 pro-inflammatory macrophages
M_{2b}	M_2	M2 anti-inflammatory macrophages
N_{0b}		Unactivated neutrophils
N_b		Activated neutrophils
	N	Neutrophils
	AN	Apoptotic neutrophils
	R	Repair mediators

Table 1: State variables for the model. Variables in both columns represent cells or mediators that diffuse between the two compartments.

Name	Description	Range used
$a_{b\infty}$	Relative effectiveness of a_b at inhibiting M_{0b} differentiation to M_{1b}	$[0.29, 67.35]$
a_∞	Relative effectiveness of a at inhibiting M_0 differentiation to M_1	$[0.13, 72.08]$
b_d	Baseline decay of damaged cells	$[1.06 \times 10^{-5}, 0.07]$
b_p	Baseline self-resolving repair of epithelial cells	$[6.72 \times 10^{-70}, 6.20]$
b_r	Baseline repair of damaged cells	$[9.79 \times 10^{-3}, 4.47]$
d_a	Rate of diffusion for a	$[0.19, 177.98]$
d_p	Rate of diffusion for p	$[0.34, 2.3 \times 10^3]$
d_{m0}	Rate of diffusion for M_0	$[0.24, 275.55]$
d_{m1}	Rate of diffusion for M_1	$[2.75 \times 10^{-3}, 19.8]$
d_{m2}	Rate of diffusion for M_2	$[0.14, 143.36]$
k_{am1}	Production rate of a by M_{1b} & M_1	$[0.01, 18.01]$
k_{am2}	Production rate of a by M_{2b} & M_2	$[2.43 \times 10^{-3}, 1.67]$
k_{an}	Rate at which neutrophils become apoptotic	$[0.01, 50.04]$
k_{anm1}	Rate of M_1 phagocytosis of AN	$[1.32 \times 10^{-3}, 0.69]$
k_{anm2}	Rate of M_2 phagocytosis of AN	$[2.71 \times 10^{-3}, 7.36]$
k_{em1}	Rate of phagocytosis of damaged cells by M_1	$[0.01, 16.03]$
k_{en}	Rate of phagocytosis of damaged cells by N	$[0.01, 16.03]$
k_{ep}	Rate of self-resolving repair mediated by p	$[5.38 \times 10^{-71}, 4.30]$
k_{er}	Rate of repair of damaged cells by R	$[1.47 \times 10^{-3}, 1.08]$
x_{er}	Regulates effectiveness of repair of damaged cells by R (Hill-type constant)	$[7.23 \times 10^{-3}, 4.13]$
k_{m0a}	Rate of differentiation of M_0 by a	$[0.01, 89.07]$
x_{m0a}	Regulates effectiveness of differentiation of M_0 by a (Hill-type constant)	$[0.16, 136.83]$
k_{m0ab}	Rate of differentiation of M_{0b} by a_b	$[1.15, 436.59]$
x_{m0ab}	Regulates effectiveness of a_b differentiation of M_{0b} (Hill-type constant)	$[0.16, 83.97]$
k_{m0ad}	Rate of recruitment of M_{0b} by a_b	$[0.34, 181.89]$
x_{m0ad}	Regulates effectiveness of recruitment of M_{0b} by a_b (Hill-type constant)	$[0.01, 27.6]$
k_{m0p}	Rate of differentiation of M_0 by p	$[8.99 \times 10^{-3}, 37.2]$
x_{m0p}	Regulates effectiveness of differentiation of M_0 by p (Hill-type constant)	$[1.17, 1.14 \times 10^4]$
k_{m0pb}	Rate of differentiation of M_{0b} by p_b	$[0.05, 89.96]$
x_{m0pb}	Regulates effectiveness of differentiation of M_{0b} by p_b (Hill-type constant)	$[41.51, 2.92 \times 10^4]$
k_{m0pd}	Rate of recruitment of M_{0b} by p_b	$[4.57 \times 10^{-3}, 53.97]$
x_{m0pd}	Regulates effectiveness of recruitment of M_{0b} by p_b (Hill-type constant)	$[0.24, 180.74]$
k_{m1p}	Rate of recruitment of M_{1b} by p_b	$[0.2, 92.81]$
x_{m1p}	Regulates effectiveness of recruitment of M_{1b} by p_b (Hill-type constant)	$[9.8 \times 10^{-3}, 1.69]$
k_{m2a}	Upregulation of M_{2b} recruitment by a	$[0.1, 219.93]$
x_{m2a}	Regulates effectiveness of M_{2b} recruitment by a (Hill-type constant)	$[0.08, 94.84]$
k_{m2r}	Upregulation of M_{2b} recruitment by R	$[3.61 \times 10^{-3}, 20.11]$
x_{m2r}	Regulates effectiveness of M_{2b} recruitment by R (Hill-type constant)	$[0.01, 18.70]$
k_{man}	Rate of M_1 switch to M_2 by AN	$[0.01, 27.08]$
k_{mne}	Rate of collateral damage to epithelial cells by macrophages and neutrophils	$[1.12 \times 10^{-3}, 5.17]$
x_{mne}	Regulates effectiveness of macrophages and neutrophils to damage epithelial cells (Hill-type constant)	$[0.03, 41.06]$
k_n	Rate of migration of N_b to lung	$[2.39 \times 10^{-3}, 3.54]$
k_{n0p}	Rate of activation of N_b by p	$[0.01, 5.58]$
x_{n0p}	Regulates effectiveness of activation of N_b by p (Hill-type constant)	$[0.03, 142.56]$
k_{pe}	Production rate of p by E_d	$[44.02, 1.12 \times 10^4]$
k_{pm1}	Production rate of p by M_1 & M_{1b}	$[0.24, 412.22]$
k_{pn}	Production rate of p and p_b by neutrophils	$[1.67 \times 10^{-3}, 2.95]$
k_{rm2}	Production rate of R by M_2	$[0.02, 40.97]$
μ_a	Decay rate of a	$[5.16 \times 10^{-4}, 5.08]$
μ_{ab}	Decay rate of a_b	$[0.04, 12.86]$
μ_p	Decay rate of p	$[2.76 \times 10^{-3}, 41.04]$
μ_{pb}	Decay rate of p_b	$[4.79 \times 10^{-4}, 3.71]$
μ_{m0}	Decay rate of M_0	$[0.01, 42.67]$
μ_{m0b}	Decay rate of M_{0b}	$[7.66 \times 10^{-3}, 329.59]$
μ_{m1}	Decay rate of M_1	$[8.2 \times 10^{-3}, 10.16]$
μ_{m1b}	Decay rate of M_{1b}	$[0.03, 60.32]$
μ_{m2}	Decay rate of M_2	$[0.27, 135.37]$
μ_{m2b}	Decay rate of M_{2b}	$[0.02, 16.51]$
μ_{nb}	Decay rate of N_b	$[2.49 \times 10^{-3}, 6.03]$
μ_{n0b}	Decay rate of N_{0b}	$[3.94 \times 10^{-6}, 2.1 \times 10^{-3}]$
μ_n	Decay rate of N	$[8 \times 10^{-3}, 4.32]$
μ_R	Decay rate of R	$[0.72, 761.75]$
s_a	Source rate of background a_b	$[5.75 \times 10^{-3}, 1.11]$
s_d	Rate of damage from ventilator	0.75
s_m	Source rate of M_{0b}	$[1.28, 1.14 \times 10^3]$
s_n	Source rate of N_{0b}	$[0.22, 225.45]$
s_p	Source rate of background p_b	$[6.5 \times 10^{-4}, 9.4]$

Table 2: Model parameters with short descriptions and ranges used in LHS.

2.4.1. Epithelial cells

We continue with the convention of three subpopulations of epithelial cells, as in Equations (6) and (7) with $E_e = 1 - E_h - E_d$. We add more details in Equations (8), (9), and (10) to describe interactions with the immune response variables that we now explicitly model for a more accurate representation of the response to VILI. The first term in Equation (8) is logistic given $E_e = 1 - E_h - E_d$, representing epithelial cells that spread and replicate to fill the empty space left by dead epithelial cells (Crosby and Waters, 2010; Gardner et al., 2010; Herold et al., 2011). This term appears negated in Equation (9) modeling the removal of the empty space. The next term in Equation (8) and the first term of Equation (9) represents repair of damaged cells back to a healthy state. Epithelial cells are prone to self-repair (Crosby and Waters, 2010), represented by a baseline rate b_r, and repair at a faster rate in the presence of repair mediators R such as chemokines, fibronectin, and other epithelial growth factors (Gordon, 2003; Herold et al., 2011; Robb et al., 2016). The third term in Equation (8) and second in Equation (9) represents collateral damage to epithelial cells by the influx and activity of the immune and is modeled via a nonlinear term, which is dependent on macrophages and neutrophils levels (Aggarwal et al., 2014; Kumar and Sharma, 2010; Nathan, 2006). We also model damage due to stretch as $s_d E_h$, the fourth term in Equation (8) and fifth term in Equation (9), in which injury occurs at a rate proportional to the amount of healthy epithelial cells at a given time.

$$\frac{dE_h}{dt} = \overbrace{(b_p + k_{ep}p)(E_h + E_d)E_e}^{\text{Proliferation of healthy cells, upregulated by PIM}} + \overbrace{E_d\left(b_r\right.}^{\text{Baseline repair}} + \left.\overbrace{\frac{k_{er}R}{x_{er} + R}}^{\text{Upregulation via repair mediators}}\right)$$
$$- \overbrace{E_h\left(\frac{k_{mne}(M_1 + N)^2}{x_{mne}^2 + (M_1 + N)^2}\right)}^{\text{Damage via M1 \& neutrophils}} - \overbrace{s_d E_h}^{\text{Damage from ventilator}} \tag{8}$$

$$\frac{dE_d}{dt} = -\overbrace{E_d\left(b_r\right.}^{\text{Baseline repair}} + \overbrace{\left.\frac{k_{er}R}{x_{er}+R}\right)}^{\text{Upregulation via repair mediators}} + \overbrace{E_h\left(\frac{k_{mne}(M_1+N)^2}{x_{mne}^2+(M_1+N)^2}\right)}^{\text{Damage via M1 \& neutrophils}}$$

$$-\overbrace{k_{em1}M_1E_d}^{\text{Phagocytsis of damaged cells by M1}}\overbrace{\left(\frac{1}{1+\left(\frac{a}{a_\infty}\right)^2}\right)}^{\text{Inhibition by AIM}} - \overbrace{k_{en}NE_d}^{\text{Phagocytsis of damaged cells by N}} + \overbrace{s_dE_h}^{\text{Damage from ventilator}} - \overbrace{b_dE_d}^{\text{Death}} \tag{9}$$

$$\frac{dE_e}{dt} = -\overbrace{(b_p+k_{ep}p)(E_h+E_d)E_e}^{\text{Proliferation of healthy cells, upregulated by PIM}} + \overbrace{k_{em1}M_1E_d}^{\text{Phagocytsis of damaged cells by M1}}\overbrace{\left(\frac{1}{1+\left(\frac{a}{a_\infty}\right)^2}\right)}^{\text{Inhibition by AIM}}$$

$$+\overbrace{k_{en}NE_d}^{\text{Phagocytsis of damaged cells by N}} + \overbrace{b_dE_d}^{\text{Death}} \tag{10}$$

M1 macrophages and neutrophils clear debris from the inflammation site to make room for healthy epithelial cells to divide and fill the empty space (Crosby and Waters, 2010; Gardner et al., 2010; Kolaczkowska and Kubes, 2013). The third and fourth terms in Equation (9) represents this phagocytosis of damaged cells by M1 macrophages and activated neutrophils, respectively. Regulation of M1 is modeled by the last multiplier in the term, representing inhibition by anti-inflammatory mediators such as IL-10 produced by M2 macrophages (Aggarwal et al., 2014; Herold et al., 2011; Johnston et al., 2012). The negative feedback loop of AIM inhibiting further pro-inflammatory functions occurs frequently in our model in a number of equations described below, and we will heretofore refer to this multiplier as inhibition by AIM. Depending on the compartment, the term may include utilize the variable a_b (bloodstream) or a (local). The anti-inflammatory and regulatory role of M2 macrophages and the balance between M1 and M2 phenotypes is critical for a successful and rapid recovery (Herold et al., 2011; Wang et al., 2014). The last term of Equations (9) and (10), b_dE_d, represents a baseline decay rate of damaged cells.

Dead epithelial cells and "empty" space are grouped together and modeled by the variable E_e in Equation (10). In the epithelial-only model, E_e was modeled as $1 - E_h - E_d$. Since mass in conserved in these three equations (the sum of terms in the epithelial differential equations is zero), E_e can be modeled either explicitly, as we chose in Equation (10), or in terms of E_h and E_d.

2.4.2. Pro- and anti-inflammatory mediators

As a signal to other immune cells, damaged epithelial cells release pro-inflammatory cytokines and other mediators, including TNF-α and matrix metalloproteinases (MMPs) (Crosby and Waters, 2010; Gardner et al., 2010; Mosser and Edwards, 2008). In our equations, we group these pro-inflammatory mediators (PIM) into two state variables: p in the lungs and p_b in the blood. The release of PIM by damaged epithelial cells leads to diffusion of PIM into the bloodstream to recruit additional immune cells (Gardner et al., 2010). This movement between model compartments is driven by their difference in concentrations in both Equations (11) and (12). This simple diffusion term will be used for other variables throughout our model.

M1 macrophages produce PIM, which upregulate the activation and migration of macrophages to the site of injury; see the second term in Equations (11) and (12) (Herold et al., 2011; Mosser and Edwards, 2008). The macrophage population self-regulates by releasing anti-inflammatory mediators (AIM) such as IL-10, thus inhibiting further production of PIM (Maiti et al., 2014). Therefore the term includes the same inhibiting multiplier as in Equation (9), through which the rate of PIM production by M1 macrophages decreases with increased concentrations of a_b.

Neutrophils are also important producers of pro-inflammatory mediators such as TNF-α, IL-1, IL-6, LTB4, and chemokines, which stimulate the activation of macrophages toward an M1 phenotype (Grommes and Soehnlein, 2011; Kumar and Sharma, 2010; Kolaczkowska and Kubes, 2013; Robb et al., 2016; Summers et al., 2010). Low levels of PIM exist in the absence of damage, accounted for by the source term s_p, and we also model natural decay of these mediators.

$$\frac{dp_b}{dt} = \overbrace{d_p(p - p_b)}^{\text{Diffusion}} + \overbrace{k_{pm1}M_{1b}}^{\text{Production via M1}} \overbrace{\left(\frac{1}{1 + \left(\frac{a_b}{a_{b\infty}}\right)^2}\right)}^{\text{Inhibition by AIM}} + \overbrace{k_{pn}N_b}^{\text{Production via neutrophils}} + \overbrace{s_p}^{\text{Background production}} - \overbrace{\mu_{p_b}p_b}^{\text{Decay}} \tag{11}$$

$$\frac{dp}{dt} = \overbrace{-d_p(p-p_b)}^{\text{Diffusion}} + \overbrace{k_{pm1}M_1}^{\text{Production via M1}} \overbrace{\left(\frac{1}{1+\left(\frac{a}{a_\infty}\right)^2}\right)}^{\text{Inhibition by AIM}} + \overbrace{k_{pn}N}^{\text{Production via neutrophils}}$$
$$+ \overbrace{k_{pe}E_d}^{\text{Production via ep. damage}} - \overbrace{\mu_p p}^{\text{Decay}} \tag{12}$$

Anti-inflammatory mediators, represented by Equation (13) in the bloodstream and Equation (14) at the site of damage, such as the anti-inflammatory signaling caused by IL-4 and IL-10 (Opal and DePalo, 2000). They follow the same simple diffusion behavior as PIM, shown by the first term in each equation below. AIM are released by both M1 and M2 macrophages (Herold et al., 2011; Johnston et al., 2012; Mosser and Edwards, 2008). Similarly to p_b, background levels of a_b are present in the absence of an immune response, represented by term four in Equation (13). Natural decay of AIM is accounted for by the last term in each equation.

$$\frac{da_b}{dt} = \overbrace{d_a(a-a_b)}^{\text{Diffusion}} + \overbrace{k_{am1}M_{1b}}^{\text{Production via M1}} + \overbrace{k_{am2}M_{2b}}^{\text{Production via M2}} + \overbrace{s_a}^{\text{Background production}} - \overbrace{\mu_{a_b}a_b}^{\text{Decay}} \tag{13}$$

$$\frac{da}{dt} = \overbrace{-d_a(a-a_b)}^{\text{Diffusion}} + \overbrace{k_{am1}M_1}^{\text{Production via M1}} + \overbrace{k_{am2}M_2}^{\text{Production via M2}} - \overbrace{\mu_a a}^{\text{Decay}} \tag{14}$$

2.4.3. Macrophages

Undifferentiated macrophages, also called naive or unactivated, are present both locally and in the blood. The diffusion term, seen in Equations (15) and (16), represents movement between compartments, modeled in the same manner as in previous equations. Increased PIM and AIM levels cause undifferentiated macrophages in the bloodstream to be recruited at a higher rate to the damaged site, where they become activated and perform phagocytic, pro-inflammatory, and pro-resolving roles (Mosser and Edwards, 2008). This increased flux between compartments due to the presence of p_b and a_b is modeled by adding terms to d_{m0} such that the Michaelis-Menten-type nonlinearity prevents this rate from increasing in an uncontrolled manner.

The equations also account for early activation in the bloodstream by PIM and AIM given a high enough concentration of these mediators (Aggarwal et al., 2014). Although there is still debate on the types of macrophages that exist in the bloodstream after being released from the bone marrow, there is evidence that populations of both M1 and M2 exist in the bloodstream before being recruited to the site of

injury (Johnston et al., 2012; Mosser and Edwards, 2008). Thus, we include this process in our equations in the second terms of Equations (15) and (16). Undifferentiated macrophages in the bloodstream can change phenotype to M1 or M2 after interacting with PIM or AIM, respectively, modeled by a Hill-type term. This nonlinearity accounts for the sufficient amount of PIM or AIM necessary to precipitate activation as well as a restriction on the rate of activation due to limited receptors on the macrophage surface.

Once pro-inflammatory mediators such as TNF-α, TGF-β, and interleukins (ILs) (Gardner et al., 2010) are released by damaged epithelial cells, undifferentiated macrophages receive these signals and differentiate into the M1 phenotype (Vlahakis et al., 1999). A pro-inflammatory response characterizes the early stages of the immune response (Herold et al., 2011; Robb et al., 2016). The second term in Equations 15 and 16 represent activation of undifferentiated macrophages to the pro-inflammatory phenotype, downregulated by the anti-inflammatory response through an inhibition multiplier. Also in this term, M2 macrophages can also be activated directly from the naive phenotype by various repair and anti-inflammatory mediators such as TGF-β and proteases involved in the repair of epithelial cells (Gardner et al., 2010; Herold et al., 2011).

Using the same inhibition multiplier as previously, AIM inhibit differentiation to M1 as part of their regulatory role in the inflammatory process, although a complete understanding of these mechanisms is yet to be uncovered (Gardner et al., 2010; Maiti et al., 2014; Mosser and Edwards, 2008). In the absence of injury, lungs contain a low number of undifferentiated macrophages which patrol the surrounding area (Crosby and Waters, 2010). "Patrolling" macrophages are also prevalent in the bloodstream. The third term in Equation (15) represents a constant source of undifferentiated macrophages from the circulation (Herold et al., 2011). We also account for natural decay of all macrophage phenotypes in Equations (15) through (20).

$$\frac{dM_{0b}}{dt} = \overbrace{(M_0 - M_{0b})\left(d_{m0} + \frac{k_{m0pd}p_b}{x_{m0pd} + p_b} + \frac{k_{m0ad}a_b}{x_{m0ad} + a_b}\right)}^{\text{Diffusion, upregulated by PIM \& AIM}}$$
$$- \; M_{0b}\left[\overbrace{\left(\frac{k_{m0pb}p_b^2}{x_{m0pb}^2 + p_b^2}\right)}^{\text{Differentiation to M1 via PIM}}\overbrace{\left(\frac{1}{1 + \left(\frac{a_b}{a_{b\infty}}\right)^2}\right)}^{\text{Inhibition by AIM}} + \overbrace{\left(\frac{k_{m0ab}a_b^2}{x_{m0ab}^2 + a_b^2}\right)}^{\text{Differentiation to M2}}\right]$$
$$+ \; \overbrace{s_m}^{\text{Source}} - \overbrace{\mu_{M0_b}M_{0b}}^{\text{Decay}} \tag{15}$$

$$\frac{dM_0}{dt} = \overbrace{-(M_0 - M_{0b})\left(d_{m0} + \frac{k_{m0pd}p_b}{x_{m0pd} + p_b} + \frac{k_{m0ad}a_b}{x_{m0ad} + a_b}\right)}^{\text{Diffusion, upregulated by PIM \& AIM}}$$
$$- M_0\left[\overbrace{\left(\frac{k_{m0p}p^2}{x_{m0p}^2 + p^2}\right)}^{\text{Differentiation to M1 via PIM}}\overbrace{\left(\frac{1}{1 + \left(\frac{a}{a_\infty}\right)^2}\right)}^{\text{Inhibition by AIM}} + \overbrace{\left(\frac{k_{m0a}a^2}{x_{m0a}^2 + a^2}\right)}^{\text{Differentiation to M2}}\right]$$
$$- \overbrace{\mu_{M_0}M_0}^{\text{Decay}} \tag{16}$$

Similarly to naive macrophages, M1 macrophages move between compartments. The presence of pro-inflammatory mediators, which act as recruiters, increases the rate of diffusion, shown in the first term of Equation (17) (Mosser and Edwards, 2008). The second term represents differentiation from the naive state, as described above.

Macrophages exhibit high plasticity, and based on the mediators and other immune cells they encounter, they can switch phenotype and perform different or enhanced functions; this plasticity is not yet fully understood (Aggarwal et al., 2014; Herold et al., 2011). M1 macrophages are primarily responsible for producing PIM, thereby recruiting other immune cells to the damaged area (Johnston et al., 2012). M2 macrophages are considered pro-resolving and downregulate PIM. Both M1 and M2 macrophages phagocytize apoptotic cells such as neutrophils (Robb et al., 2016). The shift from an overall pro-inflammatory phase to an anti-inflammatory phase in the course of the immune response is highly dependent upon a shift in macrophage behavior, specifically the shift from a mainly M1 response to a mainly M2 response

(Gardner et al., 2010; Johnston et al., 2012; Mosser and Edwards, 2008).

One of the primary ways this shift is achieved is through the inhibition of M0 to M1 differentiation by anti-inflammatory mediators, as described previously. Additionally, when pro-inflammatory macrophages phagocytize apoptotic neutrophils, they shift towards a more anti-inflammatory phenotype through suppression of the release of pro-inflammatory mediators and production of pro-resolving mediators (Kumar and Sharma, 2010; Nathan, 2006). We account for this shift by including the third term in Equation (18), proportional to apoptotic neutrophil phagocytosis which causes M1 macrophages to shift to the M2 phenotype. This term also includes inhibition of M1 function by AIM. It has been shown in some studies that M2 macrophages can switch to an M1 phenotype (Heusinkveld et al., 2011), although this idea is not currently widely accepted. Thus, we choose to include only the shift from M1 to M2.

$$\begin{aligned}\frac{dM_{1b}}{dt} =& \overbrace{(M_1 - M_{1b})\left(d_{m1} + \frac{k_{m1p}p_b}{x_{m1p} + p_b}\right)}^{\text{Diffusion, upregulated by PIM}} \\ &+ M_{0b}\overbrace{\left(\frac{k_{m0pb}p_b^2}{x_{m0pb}^2 + p_b^2}\right)}^{\text{Differentiation to M1}}\overbrace{\left(\frac{1}{1 + \left(\frac{a_b}{a_{b\infty}}\right)^2}\right)}^{\text{Inhibition by AIM}} - \overbrace{\mu_{M1_b}M_{1b}}^{\text{Decay}}\end{aligned} \tag{17}$$

$$\begin{aligned}\frac{dM_1}{dt} =& -\overbrace{(M_1 - M_{1b})\left(d_{m1} + \frac{k_{m1p}p_b}{x_{m1p} + p_b}\right)}^{\text{Diffusion, upregulated by PIM}} \\ &+ M_0\overbrace{\left(\frac{k_{m0p}p^2}{x_{m0p}^2 + p^2}\right)}^{\text{Differentiation to M1 via PIM}}\overbrace{\left(\frac{1}{1 + \left(\frac{a}{a_\infty}\right)^2}\right)}^{\text{Inhibition by AIM}} \\ &- \overbrace{k_{man}(k_{anm1}ANM_1)}^{\text{M1 switch to M2 by phagocytosis}}\overbrace{\left(\frac{1}{1 + \left(\frac{a}{a_\infty}\right)^2}\right)}^{\text{Inhibition by AIM}} - \overbrace{\mu_{M_1}M_1}^{\text{Decay}}\end{aligned} \tag{18}$$

M2 macrophages, associated with an anti-inflammatory response, can be activated directly from undifferentiated macrophages by specific anti-inflammatory sig-

nals in addition to switching phenotype from M1. They diffuse between compartments as illustrated previously, shown in the first terms in Equations (19) and (20). M2 macrophages produce anti-inflammatory mediators which recruit and promote differentiation to more M2 macrophages, described in the second term of both equations. They release cytokines that trigger the repair phase of the immune response (Herold et al., 2011; Mosser and Edwards, 2008). This repair phase includes repair mediators (discussed below in Equation (25)), which play a direct role in the reconstruction of healthy epithelial cells and resolution of damage (Herold et al., 2011).

$$\frac{dM_{2b}}{dt} = \overbrace{(M_2 - M_{2b})\left(d_{m2} + \frac{k_{m2r}R}{x_{m2r} + R} + \frac{k_{m2a}a}{x_{m2a} + a}\right)}^{\text{Diffusion}} + \overbrace{M_{0b}\left(\frac{k_{m0ab}a_b^2}{x_{m0ab}^2 + a_b^2}\right)}^{\text{Differentiation to M2}} - \overbrace{\mu_{M2_b}M_{2b}}^{\text{Decay}} \tag{19}$$

$$\frac{dM_2}{dt} = -\overbrace{(M_2 - M_{2b})\left(d_{m2} + \frac{k_{m2r}R}{x_{m2r} + R} + \frac{k_{m2a}a}{x_{m2a} + a}\right)}^{\text{Diffusion}} + \overbrace{M_0\left(\frac{k_{m0a}a^2}{x_{m0a}^2 + a^2}\right)}^{\text{Differentiation to M2}} + \overbrace{k_{man}(k_{anm1}ANM_1)}^{\text{M1 switch to M2 by phagocytosis}}\overbrace{\left(\frac{1}{1 + \left(\frac{a}{a_\infty}\right)^2}\right)}^{\text{Inhibition by AIM}} - \overbrace{\mu_{M_2}M_2}^{\text{Decay}} \tag{20}$$

2.4.4. Neutrophils

Neutrophils are considered the first responders to injury (Gardner et al., 2010; Grommes and Soehnlein, 2011). Generated in the bone marrow (Kolaczkowska and Kubes, 2013), free-flowing neutrophils circulate in the vasculature at baseline levels, described as N_{0b} and represented by the first term in Equation (21) (Grommes and Soehnlein, 2011). In the presence of injury, neutrophils are activated and recruited to the damaged site through pro-inflammatory mediators such as TNF-α, IL-1β, and other chemokines and cytokines (Grommes and Soehnlein, 2011; Summers et al., 2010). This recruitment is represented by the first term in Equations (21) and (22). On the other hand, anti-inflammatory mediators, including macrophage-produced resolvins and protectins, inhibit further recruitment of neutrophils (Nathan, 2006).

Similarly to the differentiation of macrophages, it is assumed that a higher concentration above baseline is required for neutrophils to activate, and that this activation rate saturates. Therefore, a Hill-type term with a maximum rate of k_{n0p} and a constant of x_{n0p} is used to model activation of neutrophils by PIM. To model the inhibition of neutrophil activation by AIM, we include the same inhibition multiplier as previously described. The effectiveness of these AIMs to inhibit this process is controlled by $a_{b\infty}$. We also account for intrinsic decay of neutrophils in the last term of Equations (21) through (24).

$$\frac{dN_{0b}}{dt} = -\overbrace{N_{0b}\left(\frac{k_{n0p}p_b^2}{x_{n0p}^2 + p_b^2}\right)}^{\text{Activation by PIM}}\overbrace{\left(\frac{1}{1+\left(\frac{a_b}{a_{b\infty}}\right)^2}\right)}^{\text{Inhibition by AIM}} + \overbrace{s_N}^{\text{Source}} - \overbrace{\mu_{N_{0b}}N_{0b}}^{\text{Decay}} \tag{21}$$

$$\frac{dN_b}{dt} = \overbrace{N_{0b}\left(\frac{k_{n0p}p_b^2}{x_{n0p}^2 + p_b^2}\right)}^{\text{Activation by PIM}}\overbrace{\left(\frac{1}{1+\left(\frac{a_b}{a_{b\infty}}\right)^2}\right)}^{\text{Inhibition by AIM}} - \overbrace{k_n N_b}^{\text{Migration}} - \overbrace{\mu_{N_b}N_b}^{\text{Decay}} \tag{22}$$

Neutrophils go through a multi-step process of rolling along and subsequently adhering to the surface of the endothelium. Then neutrophils transmigrate to the injury site either through or between endothelial cells (Grommes and Soehnlein, 2011; Kolaczkowska and Kubes, 2013). This process is assumed to be driven not by a concentration difference in neutrophils between the compartments but rather is a direct consequence of activation. Therefore, neutrophil transmigration, the first term in Equation (23), is modeled from the bloodstream to the site of injury by a linear term with rate k_n. Activated neutrophils also have greater longevity and their half-life increases significantly (Kolaczkowska and Kubes, 2013).

Activated neutrophils that have transmigrated through the endothelium and reached the site of injury release pro-inflammatory mediators, as discussed previously in Equation (12). During infection, neutrophils play an important role by phagocytizing pathogens (Kumar and Sharma, 2010), but during VILI a main role of neutrophils is the recruitment of macrophages, particularly to promote a more pro-inflammatory environment for the clearance of damaged and dead cells (Grommes and Soehnlein, 2011).

Neutrophils become apoptotic, modeled by the second term of Equation (23) (Gardner et al., 2010). In this state, they are phagocytized by M1 and M2 macrophages (second and third terms of Equation (24), respectively) and no longer contribute to the production of PIM (Kolaczkowska and Kubes, 2013; Soehnlein and Lindbom,

2010; Robb et al., 2016). Phagocytosis by M1 macrophages is inhibited by AIM using our standard functional form for the inhibition multiplier. AIM do not inhibit phagocytosis by M2 macrophages since AIM support the function of anti-inflammatory cells. Intrinsic decay is described in the last term of Equation (23).

$$\frac{dN}{dt} = \overbrace{k_n N_b}^{\text{Migration}} - \overbrace{k_{an} N}^{\text{Transition to apoptotic}} - \overbrace{\mu_n N}^{\text{Decay}} \tag{23}$$

$$\frac{dAN}{dt} = \overbrace{k_{an} N}^{\text{Transition to apoptotic}} - \overbrace{k_{anm1} A N M_1}^{\text{Phagocytosis by M1}} \overbrace{\left(\frac{1}{1 + \left(\frac{a}{a_\infty}\right)^2} \right)}^{\text{Inhibition by AIM}} - \overbrace{k_{anm2} A N M_2}^{\text{Phagocytosis by M2}} \tag{24}$$

2.4.5. Repair mediators

The direct contribution of alveolar macrophages to the repair of epithelial cells is not completely understood, although macrophage involvement in the repair process has been widely demonstrated (Herold et al., 2011). M2 macrophages produce various mediators that promote repair of epithelial cells. We do not model each of these explicitly, instead we group them together in one variable called R. These secreted mediators include prostaglandin E_2, chemokines such as CCL2, TGF-β, fibronectin 1 and other epithelial growth factors (Gordon, 2003; Herold et al., 2011; Robb et al., 2016). The production of R by M2 macrophages is modeled by the first term in Equation (25). The second term models intrinsic decay of these mediators.

$$\frac{dR}{dt} = \overbrace{k_{rm2} M_2}^{\text{Upregulation by M2}} - \overbrace{\mu_R R}^{\text{Decay}} \tag{25}$$

With a system of ODEs that captures the most important aspects of the immune response to VILI, the following sections demonstrate how we analyzed the model to understand the parameter space, determine the most sensitive parameters and other influential predictors of model output, and modulate particular cases of model-generated dynamics to lessen long-term epithelial damage.

2.5. Sampling method for parameters: Latin Hypercube Sampling

Because of the large number of variables and parameters, mathematical and statistical techniques need to be used to analyze the system and find parameter sets that generate biologically realistic dynamics of immune cell populations included in this

model. Some parameters are easily obtained from the literature, such as half-lives of immune cells. However, most of the parameters have not yet been evaluated due to the need for experimental data or are altogether impossible to obtain through current experimental methods. As an initial step towards determining initial conditions and parameters for this model we use Latin Hypercube Sampling (LHS). Introduced in 1979 (McKay et al., 1979), LHS is a sampling method which generates random, unique parameter sets, such that the produced parameter values are selected according to a distribution; in our case, a uniform distribution. For LHS with uniform distributions assumed for each parameter, to generate n desired parameter sets, the algorithm splits the determined range into n evenly-spaced subintervals and each interval is sampled exactly once (Marino et al., 2008). This is particularly useful for our exploratory simulations because the distributions of the parameters are unknown. Using MATLAB functions adapted from Kirschner (2008), all parameters were sampled except the rate of damage s_d due to ventilation. Lower and upper bounds were determined by starting with the same range for all parameters, covering several orders of magnitude. Within this range, we ensured that parameter sets existed which covered a variety of disease progressions and we performed additional LHS sweeps guided by these sets. Once we had parameter sets generating a wide variety of dynamics, we fixed the range to the minimum and maximum parameter values that achieved the steady-state condition (see Table 2 for values). The system of ODEs was solved with each set, and we compared transients to determine which parameter sets gave rise to biologically feasible results. First, the system ran for 800 hours without ventilator damage ($s_d = 0$) to ensure a steady-state condition was reached. Any parameter sets that did not result in an equilibrium state by 800 hours were not simulated with ventilation. The others were then run for 200 hours with damage rate nonzero for the first 2 hours, replicating experimental methods.

2.6. Cohorts: Healthy, Persistent Damage, & Dying

Simulations were separated into three categories of disease progression: 1 healthy epithelial cells sufficiently cover the alveoli to functional normally, 2) existence of persistent inflammation and associated tissue damage, and 3) a healthy epithelial cell population not large enough to survive. These progressions are called Healthy, Persistent Inflammation, and Dying, respectively.

To quantify these three different states, we divided percentages of healthy epithelial cells into categories:

- Healthy: $E_h \geq 90\%$
- Persistent inflammation: $50\% \leq E_h < 90\%$

- Dying: $5\% < E_h < 50\%$

In this way, each parameter set can be classified into three different categories based on their E_h steady-state values either before or after damage. Thus, sets are classified by their initial conditions and then again after simulation with ventilation. Cases in which $E_h < 5\%$ for the entire simulation were removed; we do not consider these biologically realistic. These parameter sets, their corresponding transients, and the outcomes they generate were used to develop a virtual cohort representing the variety of immune system dynamics generated by the model (Brown et al., 2015). The cohort was then used to compare outcomes, transient properties, underlying parameters, and their corresponding biological mechanisms.

2.7. eFAST

We use several tools to perform a sensitivity analysis of model parameters. A common method is calculating partial rank correlation coefficients (PRCCs), but results are only reliable for monotonic relationships between parameters and variables. Our model output does not fit this criteria. Marino et al. (2008) suggest the extended Fourier amplitude sensitivity test (eFAST), a variance-based method for non-linear, non-monotonic relationships. The greatest drawback of eFAST compared to PRCC is the computation time.

eFAST, developed by Saltelli et al. (2004), Saltelli and Bolado (1998), and Saltelli et al. (1999) is the extended version of FAST, originally developed by Cukier et al. (1973), Schaibly and Shuler (1973), and Collins and Avissar (1994). Parameters are varied and the resulting variation in model output is calculated using statistical variance. The algorithm varies each parameter at different frequencies by creating a sinusoidal function, called a search curve, and then sampling parameter values along the function. Fourier analysis measures the influence of the parameter's frequency on model output. First-order sensitivity S_i for a parameter i is calculated by varying only i and leaving the rest constant. Total-order sensitivity S_{Ti} is calculated by varying i using a unique, higher frequency and varying the other parameters using lower non-unique frequencies. This total-order sensitivity captures non-linear interactions between parameters in addition to changes in model output. We implement a novel method by Marino et al. (2008) to calculate S_i and S_{Ti} and determine their statistical significance of for each parameter. A "dummy parameter" is included in the parameter set and its eFAST index is compared to the other parameters found in the model.

MATLAB functions by Kirschner (2008) are available online to perform eFAST. We obtain 65 values on a search curve of each parameter and repeat this process for

five unique search curves since different ones can generate slightly different samples. Sensitivity can be calculated at specific time points for the desired variable.

2.8. Random forest decision tree

Aside from more conventional sensitivity analysis measures, we chose a few alternative methods that require less computational time and can include other features of the model besides parameters. One of these alternatives is a random forest decision tree. A decision tree algorithm is a classification tool that uses the given properties of an individual or object to determine into which category it should fall (Le, 2018; Liaw and Wiener, 2002). In this case, each parameter set in the virtual cohort has a number of predictors and outputs: parameters and any other characteristics from the transients that can be quantified or given a classification value. The algorithm takes a training set, a subset of the cohort about which all predictors and outputs are known, and can train the algorithm to classify patients into specific categories.

An output of the model that we are particularly concerned with predicting is the patient's outcome, as described in the previous section. The decision tree generated from the training set makes predictions for the rest of the virtual cohort members about whether each one will fall into one of the three outcomes: resolved to healthy, persistent inflammation, or dying. The tree contains branches at which specific parameters are chosen to best assist in classification. The parameter values of each "individual" in the cohort determines the path along the tree until it reaches the most likely outcome based on the training set.

Since a decision tree simply takes a series of values for each predictor and is not dependent on the model itself, measures besides just parameters can be used. We included supplementary predictors calculated from the transients, described in Table 3. Adding these predictors allowed for the possibility that the best classifiers of outcome could be not only parameters but also properties of the transients. This knowledge could provide additional information about metrics for experimentalists and clinicians to keep track of and identify early warning signs for undesirable results.

For added robustness against overfitting (**?**), we use a random forest decision tree algorithm, in which a user-specified number of randomly chosen parameters are candidates at each branch; then the algorithm selects one to be the splitting variable from that smaller group. The `rf` function in R generates 500 decision trees as the "forest" along with several other useful output metrics. One metric in particular is the importance value of each parameter or characteristic, calculated from the Gini Index. The importance value is a measure of how important any given parameter was in determining the outcome of each parameter set in the virtual cohort. Because of the large number of parameters in the model, this can provide intuition on

Predictor	Comment, description
Maximum $M1$ percent	
Maximum $M2$ percent	
Minimum $M1$ percent	
Minimum $M2$ percent	
Maximum $M1$	
Maximum $M2$	
Minimum $M1$	
Minimum $M2$	
$M1$ peak time	Time at which $M1$ peak occurs
$M2$ peak time	Time at which $M2$ peak occurs
$M2$ percent at 10 hours	
$M1$ peak ratio	Ratio of $M1$ peak to $M1$ initial condition
E_h difference	Difference between first and last time points of E_h
E_h ratio 0.5h	Ratio of IC to E_h at 30 minutes
E_h ratio 2h	Ratio of IC to E_h at 2 hours
E_h ratio 6h	Ratio of IC to E_h at 6 hours
Fits $t = 0$ $M0$ data	0 = does not fit, 1 = does fit
Fits all data	0 = does not fit, 1 = does fit

Table 3: Additional predictors used in analysis of parameter space with descriptions if necessary. These predictors were used with the random forest decision tree, correlations, and significance testing.

which parameters and other characteristics of the transients are most influential in determining outcomes.

3. Results

Our aim is to understand how recruitment of the immune response and its interactions with epithelial cells translate to specific outcomes and what dynamics are driving this process. Therefore, we developed an ODE model of the immune response to VILI, which explicitly tracks macrophage phenotype and epithelial cells. A fixed point and stability analysis of the epithelial subsystem reveals the long-term stability of a simplified version of the system under various conditions, and how changes in those conditions affect stability. Using Latin Hypercube Sampling, we generated parameter sets that replicate different possible responses to VILI and created a virtual cohort of patients. We also perform an analysis of the large parameter space by comparing various techniques to determine predictors of outcome and/or processes that could be targeted to modulate outcome.

3.1. Sample Transients and Cohort Breakdown

This model can generate a variety of dynamics, similar to expected responses to patients on a ventilator. There is significant variability between outcomes as well as within them. Figure 4 shows examples of these different dynamics for healthy epithelial cells and M0, M1, and M2 macrophages using a case of each of the three outcomes: resolved to healthy, persistent inflammation, and dying. Experimental data is shown in Figure 4 are percentages of the total amount of local macrophages.

We generated 100,000 parameter sets using LHS with parameter ranges given in Table 2. Figure 5 shows the breakdown of these parameter sets based on whether or not the dynamics lead to a steady-state system in the absence of ventilation, their classification before ventilation, and the resulting outcome after a two hour ventilation (healthy, persistent inflammation, and dying). The top number in each box is the total number of parameter sets in that category, and that number is further broken down by the category in which they start (column 1) and end (column 2). For the first column, the number in parentheses is the number of sets that started in that category but ended in a different one. Conversely, the number in parentheses in the second column shows the sets that ended in a certain outcome but did not start there. These numbers serve as a summary of how damage may affect outcome for the variety of behaviors in the virtual cohort. The table also gives a breakdown of the parameter sets that give rise to transients that fit within one standard deviation of the $M0$ data point at $t = 0$ hours, all data points at $t = 0$, and all data points for

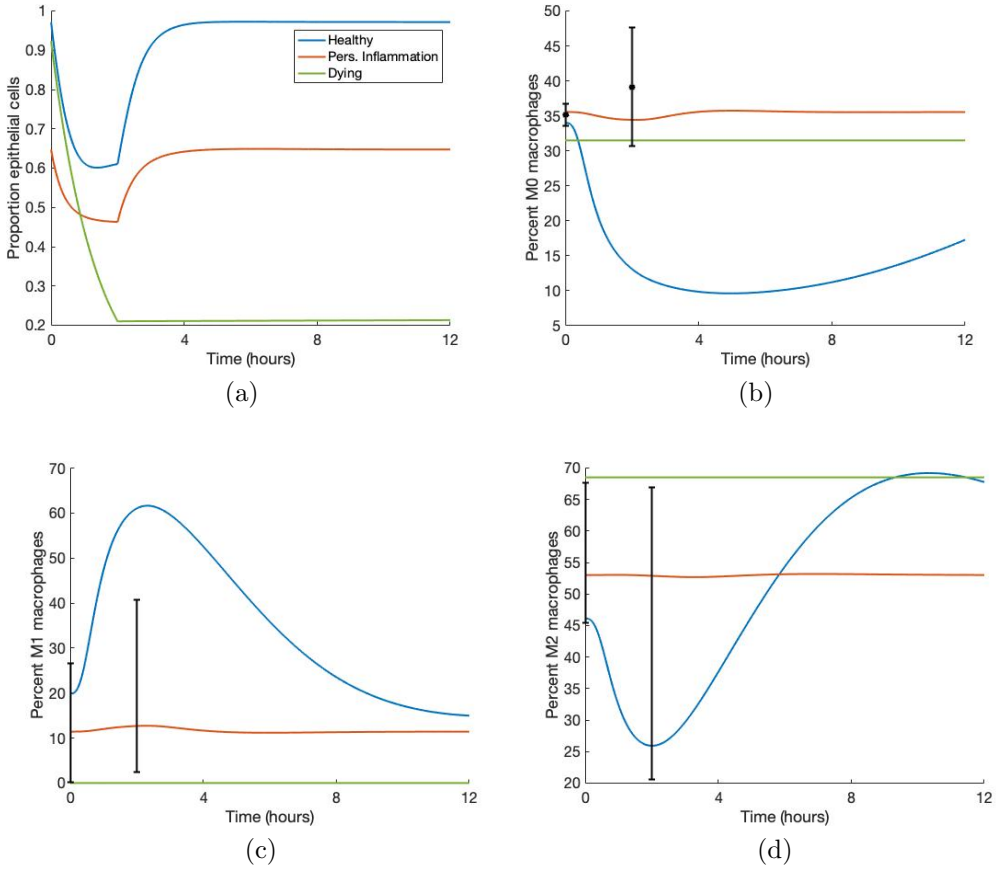

Figure 4: Sample simulations; blue, orange, and green curves indicate Healthy, Persistent inflammation and Dying outcomes, respectively. Black error bars represent data obtained as described in the Experimental methods section. (a) Proportion healthy epithelial cells. (b) Percent M0 macrophages. (c) Percent M1 macrophages. (d) Percent M2 macrophages.

$t = 0$ and 2 hours. Data is used to illustrate how using a cohort can be beneficial in generating a variety of dynamics that fit the data through unique parameter sets, but given the limited data available (few times points and only a few of the variables), we will analyze all 22,554 sets that reach steady state whether or not they fit the data to understand the full array of responses that could occur.

As seen in the example transients in Figure 4, our model generates a large range of initial conditions and dynamics. However, all of the values generated may not be biologically realistic; *in vivo* murine experimental data from may provide additional information about realistic amounts of macrophage concentration and activation. As mentioned in the description of the experimental methods, macrophages can express M1 and M2 markers at the same time. M1 and M2 variables in the model track overall M1 and M2 expression rather than quantities of cells, so we compare the data to our variables as percentages of the total number of macrophages. Many of the transients were prevented from fitting the data because of the small standard deviation for M0 data. Furthermore, the resulting M1 and M2 ranges were quite overlapped for the two time points due to their large standard deviations; thus, many transients that fit the data showed minimal activation although it is well known that M1 and M2 expression peaks considerably during and after injury (Aggarwal et al., 2014; Robb et al., 2016). For these reasons and since there are only two time points available, we focus on the first time point, specifically for naive M0 macrophages, as a starting point. Table 4 shows a breakdown of the 466 parameter sets which resulted in an M0 transient that fit the first data point.

	Starting state	Outcome	Comment
Healthy	309	301	Start healthy → end pers. inf.: 8
Pers. Inf.	109	116	Start pers. inf. → end dying: 1
Dying	48	49	

Table 4: A breakdown of the 466 total parameter sets that resulted in an M0 transient that fit the data.

Because the mice from which the samples were collected were otherwise healthy and were also sacrificed immediately after the two-hour ventilation period, their outcomes are unknown. Table 4 shows that our model generates transients that fit this data point and result in all three outcomes. In the following sections we use several analysis techniques, first considering all 22,554 sets that fit the steady-state condition, and then only the 466 sets that fit the first data point. This allows for

Total LHS runs: 100,000

Steady-state: 22,554

	IC	ES
H:	15193 (415)	14781 (3)
P:	4861 (72)	5099 (310)
D:	2500 (3)	2674 (177)

Not steady-state: 77,446

Fit, $t = 0$/M0: 466

	IC	ES
H:	309 (8)	301 (0)
P:	109 (1)	116 (8)
D:	48 (0)	49 (1)

Not a fit, $t = 0$/M0: 22,088

	IC	ES
H:	14884 (407)	14480 (3)
P:	4752 (71)	4983 (302)
D:	2452 (3)	2625 (176)

Fit all, $t = 0$: 140

	IC	ES
H:	91 (1)	90 (0)
P:	27 (1)	27 (1)
D:	22 (0)	23 (1)

Not a fit, $t = 0$: 326

	IC	ES
H:	218 (7)	211 (0)
P:	82 (0)	89 (7)
D:	26 (0)	26 (0)

Fit all, $t = 0$ & 2: 96

	IC	ES
H:	54 (1)	53 (0)
P:	15 (1)	15 (1)
D:	14 (0)	15 (1)

Not a fit, $t = 0$ & 2: 57

	IC	ES
H:	37 (0)	37 (0)
P:	12 (0)	12 (0)
D:	8 (0)	8 (0)

Figure 5: Results of 100,000 LHS runs and breakdown of their initial conditions (IC) and ending states (ES) by category healthy (H), persistent inflammation (P), or dying (D) Numbers in parentheses in the IC columns are the number of simulations that started in the category associated with that row and change their state after ventilation. Numbers in parentheses in the ES columns are the number of simulations that ended in the category associated with that row, but were not in that category before ventilation.

enough sets to analyze the results.

3.2. Determining Predictors and Driving Dynamics

Our model has 18 variables and 67 parameters. Using a variety of mathematical, statistical, and computational methods, we determined the parameters and other predictors that stand out, those to which output is most sensitive and may help differentiate or predict what is driving outcome. In this section we explain and compare the results of each method.

3.2.1. Correlations and significance testing highlight specific parameters

As an initial step towards understanding relationships between parameters and model output, we calculated the correlations of parameters and predictors with outcome. There are only a few correlations higher than $R = 0.3$; notable pairs are shown in Figure 6 using random samples of each outcome for better visibility of the points. Interestingly, the parameters b_r and k_{mne} are more correlated with the ratio between E_h at some point during ventilation and the initial E_h value than with the value of E_h at 200 hours, i.e. how we define the transient's outcome. Lower ratios imply less significant of a change in epithelial health due to ventilation. For k_{mne}, the rate of collateral damage to epithelial cells by macrophages and neutrophils, parameter sets that result in persistent inflammation and dying outcomes have a significant correlation with the same E_h ratio, shown in Figure 6a. The k_{mne} parameter has the following correlations for each type of outcome: resolved to healthy $R = 0.07$ (not shown); persistent inflammation $R = 0.59$; dying $R = 0.77$. The b_r parameter, representing the baseline repair rate for epithelial cells, has the following correlations for each type of outcome, shown in Figure 6b: resolved to healthy $R = 0.34$; persistent inflammation $R = 0.35$; dying $R = 0.12$ (not shown). Visual inspection of both graphs show possible nonlinear behavior that should be investigated further. The only other pair with a correlation above 0.3 is s_m, the source rate for naive macrophages, and the maximum and minimum values of M2 macrophages over the entire simulation. The parameter s_m and maximum M2 has the following correlations: healthy $R = 0.32$; persistent inflammation $R = 0.32$; dying $R = 0.33$. Figure 6c shows the results for s_m and maximum M2; s_m and minimum M2 is not shown but has similar results.

We also performed hypothesis testing for predictors (excluding binary variables). The Kruskal-Wallis Test is an alternative to ANOVA when the variable distributions are not normal (McKight and Najab, 2010). Due to our choice of a uniform sampling distribution for LHS, parameter distributions for the 22,554 sets are roughly uniform. We categorized all parameter sets by their outcome (healthy, persistent

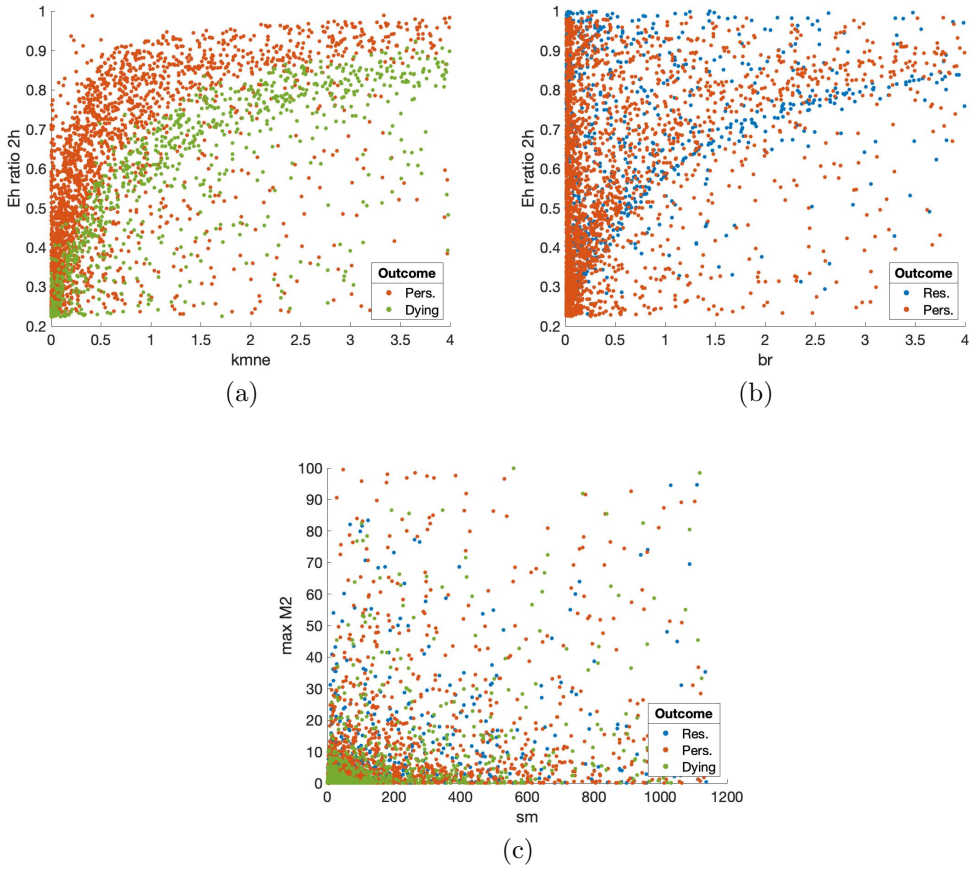

Figure 6: Scatter plot of predictors with notable correlations. Points are a random sample of the total points. (a) Parameter k_{mne} (rate of collateral damage to epithelial cells by macrophages and neutrophils) versus ratio of E_h at 30 minutes to initial E_h values. Correlations: resolved to healthy $R = 0.07$ (not shown); persistent inflammation $R = 0.59$; dying $R = 0.77$. (b) Parameter b_r (baseline rate of epithelial repair) versus ratio of E_h at 2 hours to initial E_h values. Correlations for parameter sets in each outcome: resolved to healthy $R = 0.34$; persistent inflammation $R = 0.35$; dying $R = 0.12$ (not shown). (c) Parameter s_m (source rate of M0 macrophages) versus maximum M2. Correlations for parameter sets in each outcome: resolved to healthy $R = 0.32$; persistent inflammation $R = 0.32$; dying $R = 0.33$.

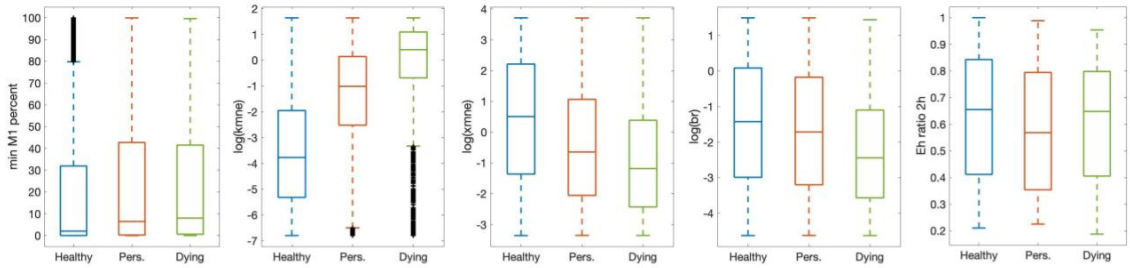

Figure 7: Subset of parameters and predictors that showed a statistically significant difference between all three outcomes: healthy, persistent inflammation, and dying, as determined by the Kruskal-Wallis and Wilcoxon Tests. Some are shown on a log scale for better visibility. Black x's are outliers.

inflammation, dying) and compared them. If any of the three groups had a statistically significant difference (p-value less than 0.01), a Wilcoxon test was performed on each pair (healthy and persistent inflammation, healthy and dying, persistent inflammation and dying) to determine which groups were different from one another. P-values for the Kruskal-Wallis and Wilcoxon tests were adjusted using the Benjamini–Hochberg procedure to control for the false discovery rate (Benjamini and Hochberg, 1995). Knowledge of which parameters and other predictors are different between groups depending on the outcome provide insight into predicting outcomes and which predictors might help influence the immune response to damage.

35 out of 81 parameters and other predictors returned results for a statistically significant difference between at least two groups and 11 gave statistically significant differences between all three groups. Table 5 shows a summary of the results from the various methods used to examine predictors significance in determining of model output. Column 1 of Table 5 shows the predictors in which all three groups were different from one another, as determined by the Kruskal-Wallis and Wilcoxon Tests. Results in columns 2-5 are described in the following sections. Box plots of a subset of predictors in which all three groups are different are shown in Figure 7 to help visualize these differences.

3.2.2. Parameter Sensitivity with eFAST

Since outcome of E_h is the metric by which we determine health of the individual, we calculated eFAST indexes for E_h at at 30 minutes, two hours (end of ventilation), and six hours. We calculated first-order and total-order sensitivities S_i and S_{Ti}, respectively. Figure 8 shows results for the parameters with $p < 0.02$. Parameters k_n (rate of migration of N_b to lung), x_{mne} (Hill-type constant for effectiveness of

All sets		Fit M0 at $t = 0h$		eFAST (Ordered)		
Sig. Testing (Not ordered)	Random Forest (Ordered output)	Sig. Testing (Not ordered)	Random Forest (Ordered output)	0.5h	2h	6h
k_{mne}	k_{mne}	k_{mne}	k_{mne}	k_n	k_n	x_{m0a}
	E_h ratio 6h	x_{mne}	x_{mne}	μ_p	x_{mne}	
x_{mne}	x_{mne}		E_h ratio 6h	x_{m0a}	k_{en}	
E_h ratio 2h	E_h ratio 2h		E_h ratio 2h	x_{mne}	b_r	
E_h ratio 0.5h	E_h ratio 0.5h		E_h ratio 0.5h	k_{en}	x_{nup}	
b_r	b_r		d_p	b_r	x_{m0a}	
	Min $M1$		a_∞	μ_{m1}	s_p	
k_{en}	k_{en}		x_{m2r}	k_{am1}	μ_p	
	k_{ep}		k_{en}		k_{pe}	
Min M1%	Min M1%		μ_{m2b}		μ_R	
μ_p						
k_{em1}						
$M1$ peak ratio						
$M1$ peak time						

Table 5: Summary of three different methods used to determine the most influential predictors, including parameters and other factors. Those that occurred most frequently are colored for better visibility. Columns 1 & 2 show results for all 22,554 parameter sets and columns 3 & 4 show results for the 466 parameters that fit the $M0$ data point at 0h. Columns 1 & 3: significance testing results for predictors in which all three outcome groups are statistically different (column 1 $p < 0.01$; column 3 $p < 0.05$). For ease of comparison between columns, the predictor is listed next to its counterpart in the random forest list, if listed in that column. Columns 2 & 4: average importance values determined by random forest decision trees. The top ten are ordered from highest to lowest importance. Columns 5-7: eFAST results (ordered by p-value, with $p < 0.02$) for three time points.

macrophages and neutrophils to damage epithelial cells), x_{m0a} (Hill-type constant for effectiveness of differentiation of M_0 by a), b_r (baseline repair of damaged cells), and k_{en} (phagocytosis of damaged cells by N) are sensitive for several time points. Comparing S_i and S_{Ti} in Figure 8, it is possible that nonlinear interaction between parameters affects model output more at 6 hours than at 2 hours. Parameters with a significant S_i may also be better candidates for treatment than those with a significant S_{Ti} because first-order sensitivity measures sensitivity of E_h based only on fluctuations in a single parameter. For this reason and since many of the same parameters are significant in for first-order and total-order sensitivity, we show results for first-order sensitivity in Columns 5-7 of Table 5, ordered from lowest p to highest and for the three time points specified.

3.2.3. Random forest algorithm to determine predictors

The randomness of the decision tree algorithm means that each random forest generated and its resulting importance values will be slightly different. To offset any unusual results generated by the randomness, we replicated the process of choosing a training set, determining the number of parameters from which to select at each branch, and generating importance values from the random forest 1000 times. Figure 9 shows the average and standard deviations of the top ten importance values generated.

Notice that the standard deviations are small enough so that although some of the top importance values may change order in different random forest simulations, in general the most important predictors will remain the same across numerous simulations. Furthermore, several of the top ten predictors except E_h difference were also found to be significant by the Kruskal-Wallis Test and b_r and k_{mne} are shared by random forest and eFAST. (see Table 5). The consistency of the importance of these predictors using different methods supports the idea that they play a significant role in determining or differentiating outcomes and the sensitivity of model output to specific parameters.

3.2.4. Analysis of parameter sets that fit data

Using the same analysis techniques as with all 22,554 parameter sets, we re-analyzed only the sets that fit the $M0$ data point at the start of ventilation ($t = 0h$) to determine if fitting any of the data provides new information. First, correlations were re-calculated with only sets that fit the first data point for the M0 variable. Correlations change slightly for each outcome, though b_r and E_h ratio, k_{mne} and E_h ratio, and s_m and M2 max/min still have consistently high correlations. Figure 10 shows these results. Correlation between k_{mne} and E_h ratio decreases slightly for the persistent inflammation outcome, from 0.59 when considering all parameter sets to

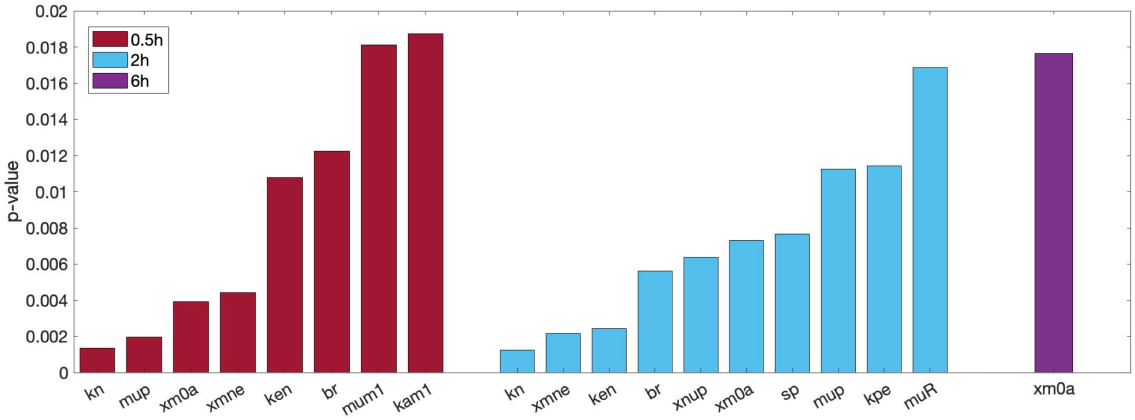

(a)

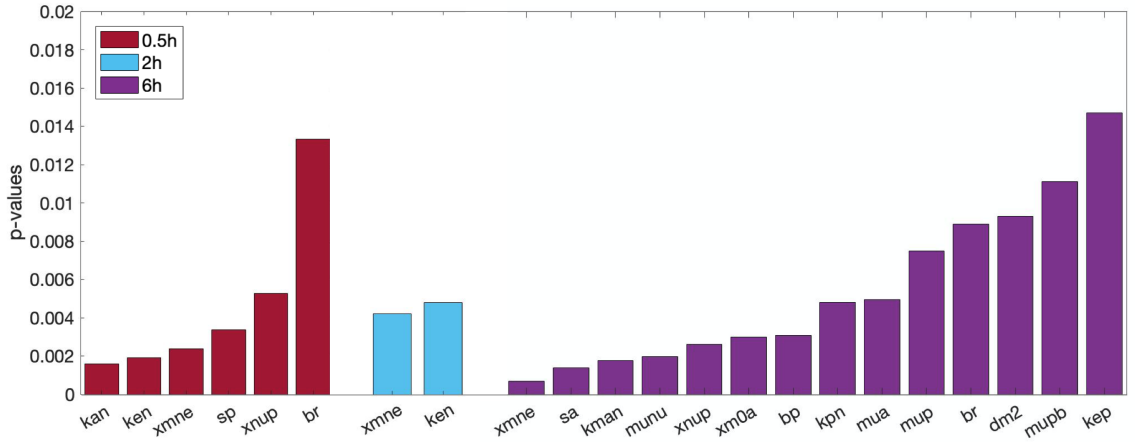

(b)

Figure 8: Parameters determined by eFAST to be most sensitive, with p-values calculated by comparing eFAST sensitivity indexes to a dummy variable. (a) First-order sensitivity, also shown in Table 5. (b) Total-order sensitivity. Results are given for each of the time points tested: 0.5 (red), 2 (blue), and 6 hours (purple).

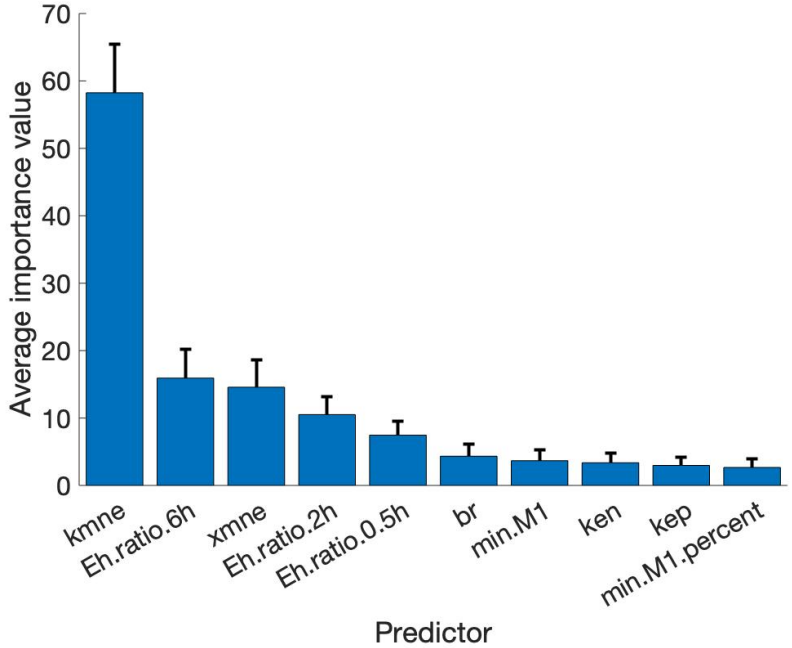

Figure 9: Mean and standard deviation of importance values for the top ten highest predictors from 1000 random forest decision trees.

0.45 for just those that fit the data, while the correlation for the healthy outcome increases slightly from 0.07 to 0.13 (Figure 10a). For b_r, shown in Figure 10b, the healthy and persistent inflammation outcome correlations are about the same and the dying outcome correlation decreases from 0.12 to 0.05. Finally, for s_m and max M2 (Figure 10c), correlation increases slightly for the healthy outcome.

We performed the Kruskal-Wallis Tests (and Wilcoxon Tests when necessary) for the parameter sets that fit the first $M0$ data point to determine which groups (healthy, persistent inflammation, dying) are statistically significantly different from one another. Only the parameters k_{mne} and x_{mne} gave results with $p < 0.05$ for a difference between all outcomes. Column 3 of Table 5 and Figure 11a show these results.

We calculated the average importance values for the parameter sets that fit the $M0/t = 0$ data point using 1000 random forests. Results are shown in Figure 11b. Six of the top ten factors from the random forest for all parameter sets are in the top ten for the selected sets.

The parameter x_{mne} increased in average importance relative to the other top importance values while the random forest algorithm determined that other parameters including d_p, a_∞, and x_{m2r} are more important for the sets that fit the first $M0$ data point. We do not perform a second eFAST sensitivity analysis since eFAST uses the model equations to calculate indexes, not parameter sets.

Table 5 shows a summary of the results from significance testing, eFAST, and random forest decision tree. Many of the same predictors are highlighted by the different methods, including E_h ratio at 0.5, 2, and 6 hours, $M1$ metrics, k_{mne}, x_{mne}, k_{en} and b_r.

3.3. Modulating recovery: a case study of select transients

Out of the 466 parameter sets that fit the first data point, nine sets result in E_h transients that start within one category of disease progression and end in another, shown in Figure 12. We used the information gained in the parameter analysis to identify key targets for treatment that could modulate damage, especially in the case of a patient starting in one state and after ventilation ending in a different, negative outcome.

Our analysis shows that the parameters b_r, the rate of self-repair of healthy epithelial cells, k_{mne}, the rate of collateral damage by macrophages and neutrophils to epithelial cells, x_{mne}, the Hill-type constant which regulates the effectiveness of macrophages and neutrophils to damage epithelial cells, and k_{en}, the rate of phagocytosis of damaged cells by neutrophils, are some of the most influential parameters and thus could inform targets for treatment. It is also important to note that differ-

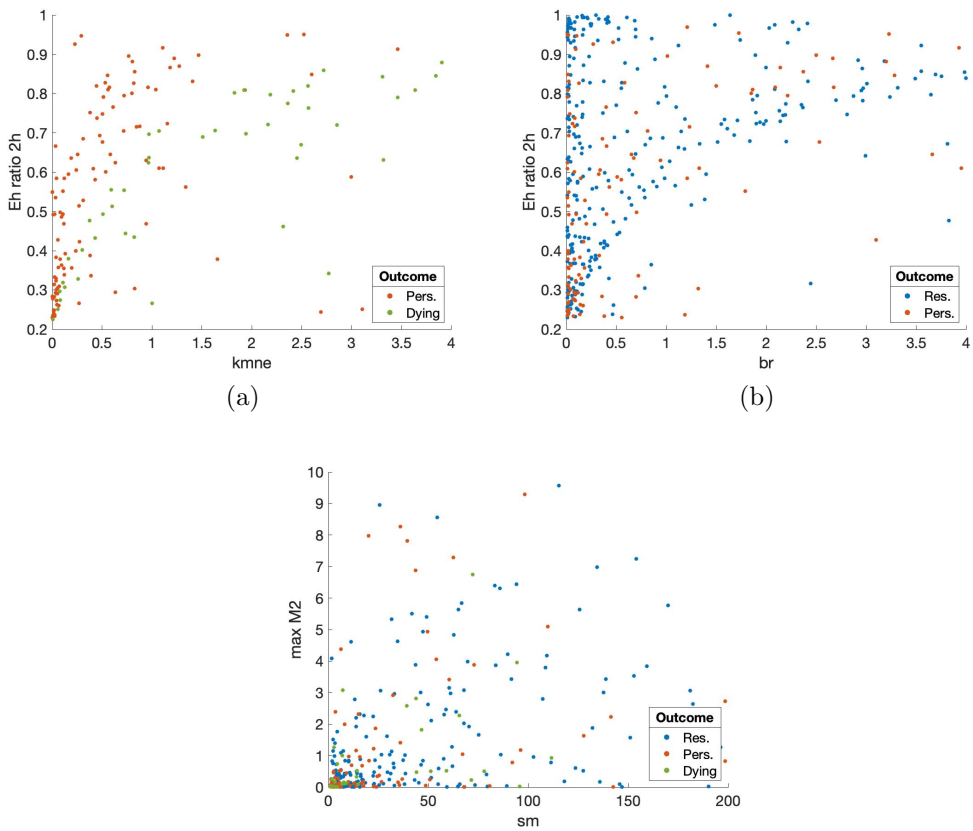

Figure 10: Scatter plots updated to include only data points that fit $M0$ data point at $t = 0$. (a) Parameter k_{mne} versus ratio of E_h at 2 hours to E_h initial condition. Correlations: resolved to healthy $R = 0.13$ (not shown), persistent inflammation $R = 0.45$, dying $R = 0.78$. (b) Parameter b_r versus same E_h ratio. Correlations: resolved to healthy $R = 0.33$, persistent inflammation $R = 0.38$, dying $R = 0.05$ (not shown). (c) Parameter s_m versus maximum M2. Correlations: resolved to healthy $R = 0.44$, persistent inflammation $R = 0.33$, dying $R = 0.30$.

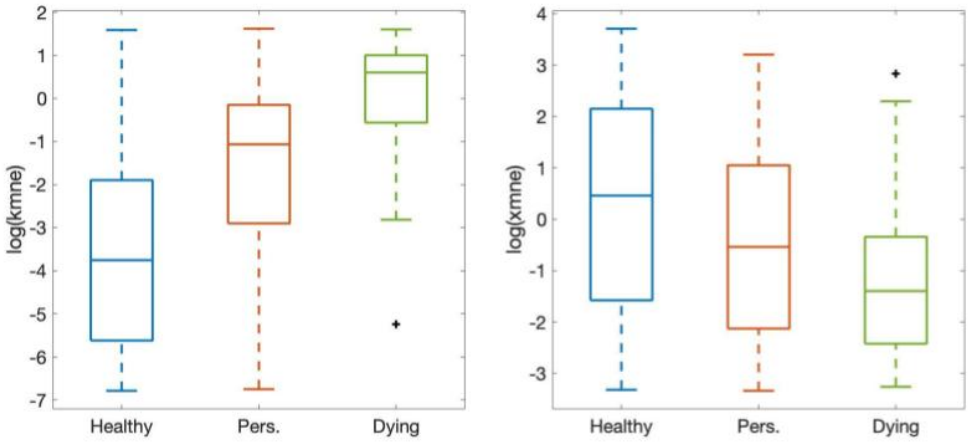

(a)

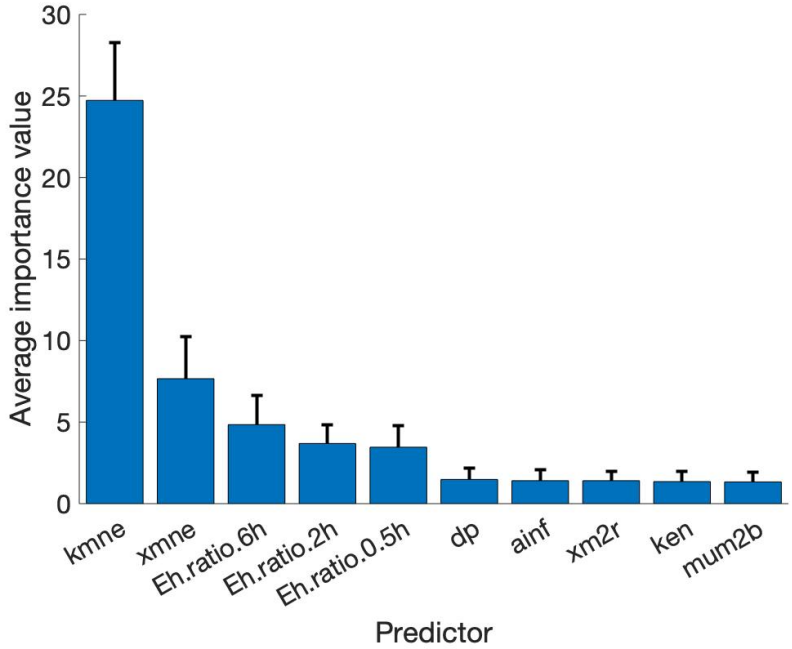

(b)

Figure 11: Results from analysis of parameter sets which generate transients that fit within one standard deviation of the $M0$ data point at the beginning of the simulation. (a) The two parameters that are statistically significantly different for all three outcomes ($p < 0.05$) based on the Kruskal-Wallis and Wilcoxon Tests. Shown on a log scale for ease of comparison. (b) Mean and standard deviation of importance values from 1000 random forests.

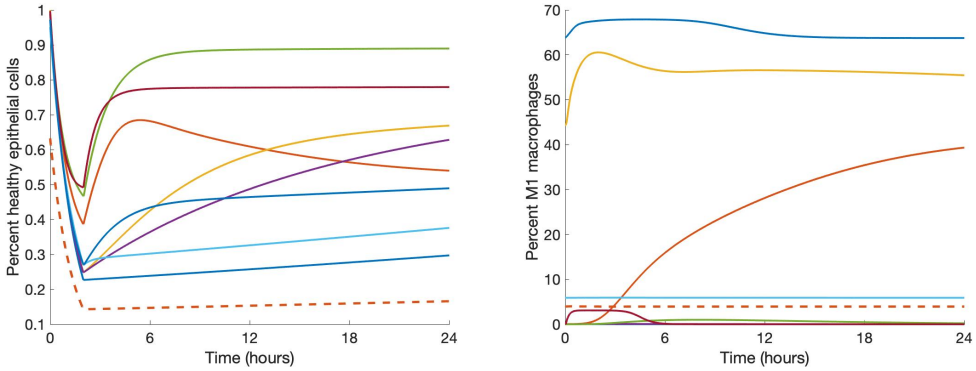

(a) (b)

Figure 12: (a) Transients of E_h that start at one state and end at a lower one. (b) Corresponding transients of $M1$. Solid lines represent transients that start healthy and ends in persistent inflammation; the dotted line represents the transient that starts in persistent inflammation and ends dying.

ent interventions could begin and end at any time during or after ventilation, so we examined interventions at several different time points (see Figure 13).

The first case in which we intervene is the one that starts healthy and ends in a persistent inflammation outcome. Note in Figure 13, the original E_h transient begins recovery to healthy after the two-hour ventilation period, but decreases to a new, lower steady-state. This is coupled with a transient for M1 in which the pro-inflammatory phenotype increases to 40-45% and stays in this range.

Increasing b_r by various amounts has increasingly positive effects on long-term epithelial health. Lower values of b_r increase the steady-state slightly and an earlier intervention can generate a higher peak of E_h around five hours, but the end steady-state is the same regardless of intervention time. If b_r is increased substantially for a significant duration of treatment time, healthy epithelial cells reach a higher steady-state value after ventilation and do not decrease again. Shown in Figures 13a and 13d, doubling b_r to 0.66 is not enough to generate recovery, but increasing b_r by a factor of four to 1.32 does result in a healthy outcome. For an insufficient treatment duration and value of b_r, levels of E_h will be higher until treatment ends and then decrease back to the same level as the original simulation. For a long enough treatment duration, the steady-state of healthy epithelial cells will remain high even after treatment ends. For $b_r = 0.66$, the intervention time does not affect health in the long run, whereas for $b_r = 1.32$, intervention at 0 and 2 hours is sufficient to bring about recovery while intervention at 4 hours is not.

The parameter k_{mne} has an inverse relationship with epithelial health; thus, decreasing the parameter provides better results. Decreasing k_{mne} slightly can increase the epithelial steady-state slightly but not enough to change the outcome to resolved. However, with a significant enough decrease of k_{mne}, M1 activation peaks around hour 10 and decreases back to its original levels whereas the original simulation shows M1 activation leveling off at a high percentage of activation (Figure 13e). The modulated return to baseline levels is paired with a healthy outcome for epithelial cells (Figure 13b). For higher values of k_{mne}, results are about the same for any intervention time 4 hours or less after the beginning of ventilation. Note in Figure 13 that the time at which intervention begins matters somewhat for changes in b_r but not for k_{mne}. Figures 13b and 13e show that half of the original value of k_{mne} (0.38 to 0.19) is not low enough to change the outcome; multiplying by a factor of 0.1 to $k_{mne} = 0.04$, on the other hand, is sufficient to change the outcome to healthy.

We also increase the parameter x_{mne}. Increasing this value causes the presence of macrophages and neutrophils to be less effective in damaging epithelial cells. Similarly to the other treatments, sufficient changes to x_{mne} bring about long-term recovery and the time at which intervention begins is not as important. Figures 13c and 13f show doubling x_{mne} to 1.85, insufficient to change the outcome, and increasing x_{mne} by a factor of four to 3.69, which is sufficient.

Finally, we increase k_{en}. This increases the rate at which neutrophils phagocytize damaged cells, making room for new, healthy cells. Interestingly, although k_{en} is shown to be an important parameter in our parameter analyses, even increasing the parameter by a factor of ten to 1.52 is insufficient to make any real changes in the epithelial and macrophage populations. Since there was no significant change, we do not show this treatment in Figure 13.

We also examine the results of combination therapy that could include regulation of two or three parameters. Together, changes in parameter values that would be insufficient on their own are able to regulate macrophage activation and bring epithelial cells back to a healthy state. Additionally, higher values of b_r and x_{mne} and lower values of k_{mne} precipitate a quicker recovery from damage. Intervention time is important for parameter values near the baseline, but not for parameter values sufficiently above or below the threshold. Intervention time may make a difference in the ending steady-state values of E_h or $M1$, depending on the parameter values. Many combinations could be formulated; Figure 14 shows two cases in which two parameter changes were insufficient to bring about recovery individually but are sufficient when combined. The orange curves show $b_r = 0.99$ and $k_{mne} = 0.19$ and the blue curves show $x_{mne} = 2.31$ and $k_{en} = 1.52$, which bring about long-term recovery

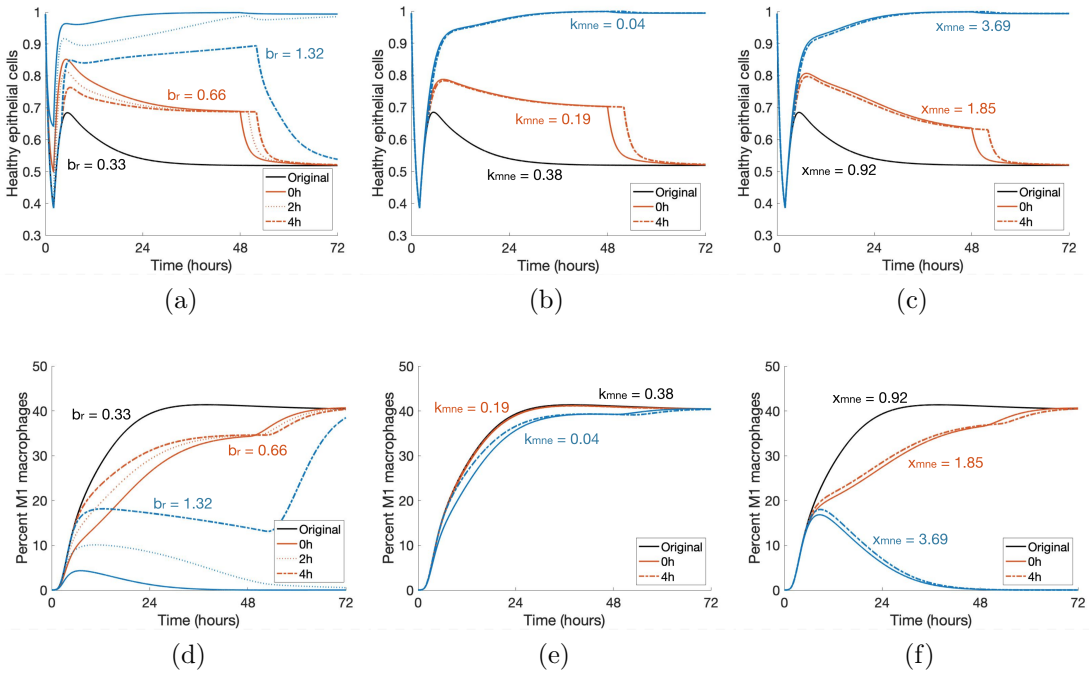

Figure 13: Starting with a parameter set that gives rise to an E_h transient that starts healthy and ends in a persistent inflammation state, we applied various treatment strategies by changing three key parameters, b_r (rate at which healthy epithelial cells self-repair), k_{mne} (rate of collateral damage to epithelial cells by macrophages and neutrophils), and x_{mne} (Hill-type constant which regulates the effectiveness of macrophages and neutrophils to damage epithelial cells). Results for various changes are shown for healthy epithelial cells (a, b, c) and percent of M1 macrophages (d, e, f). Treatment was started at 0, 2, or 4 hours after the start of ventilation, denoted by solid, dotted, and dot-dashed lines, respectively, and lasted for 48 hours. The original parameter values are $b_r = 0.33$, $k_{mne} = 0.38$, and $x_{mne} = 0.92$. Black transients show the original dynamics without intervention. Orange transients represent values of each parameter that are insufficient to mediate prolonged macrophage activation. Blue transients show values that are sufficient to bring about resolution, depending on intervention time.

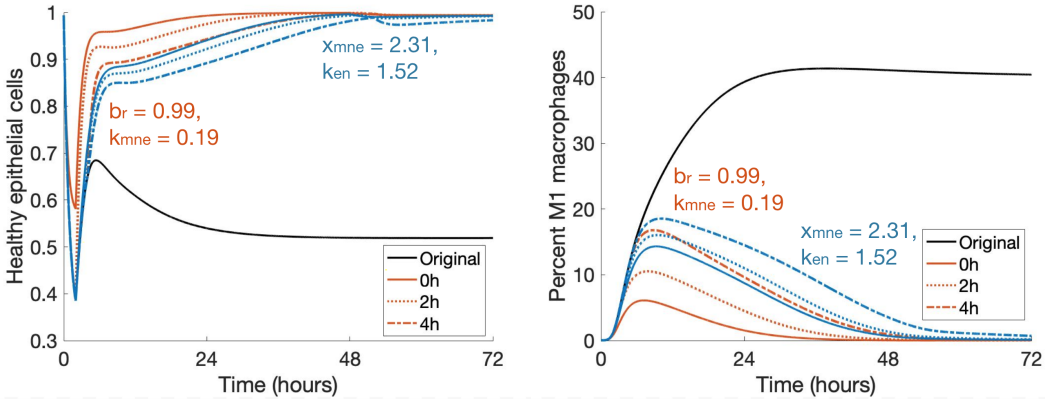

(a) (b)

Figure 14: Changes in b_r, k_{mne}, x_{mne} and k_{en} that are insufficient on their own (Figure 13) result in a change in outcome when combined. Orange curves show a combination treatment of $b_r = 0.99$ and $k_{mne} = 0.19$ and blue curves show that of $x_{mne} = 2.31$ and $k_{en} = 1.52$. Duration of treatment in each case is 48 hours, and all intervention times are successful in a long-term recovery.

for all three intervention times.

For other cases that change steady-state (those starting in a healthy state and ending in persistent inflammation or starting in persistent inflammation and ending in a dying state) a high enough b_r can bring about resolution in some cases, with earlier intervention times resulting in a higher steady-state, but there are varied responses to changes in k_{mne}, x_{mne}, and k_{en}. In fact, a higher k_{en} can be detrimental. Even for transients with similar E_h and $M1$ dynamics, reactions to treatments are very different, reinforcing the uniqueness of each individual member of the virtual cohort.

To examine different responses to treatments, we compare 48-hour treatments in two different cases: one begins in a persistent inflammation disease progression and ends in a dying state, and the other begins healthy and ends in a persistent inflammation state. We tested treatments using the four parameters from the first case study multiplied by different factors: b_r multiplied by a factor of 20, k_{mne} multiplied by a factor of 0.05, x_{mne} multiplied by a factor of 20, and k_{en} multiplied by a factor of 0.05. Additionally, since k_n was identified by eFAST as being a parameter to which E_h is sensitive, we also included k_n multiplied by a factor of 20 as a treatment.

One case, shown in Figures 15a and 15c, started with $b_r = 1.22$, $k_{mne} = 0.005$, $x_{mne} = 2.71$, $k_{en} = 2.31$, and $k_n = 0.43$. Changes to x_{mne} and k_{en} made no substantial

impact on the percentage of healthy epithelial cells; thus, they are not shown in the figures. Figure 15c shows a spike in M1 due to the change in k_n; this is paired with an increase in E_h, but after the treatment ends at the 48-hour mark, the rate of recovery of healthy epithelial cells decreases to about the same rate as that of the original transient.

The other case, shown in Figures 15b and 15d, responds differently to the treatments. Original parameter values were $b_r = 0.010$, $k_{mne} = 0.015$, $x_{mne} = 24.67$, $k_{en} = 0.011$, and $k_n = 0.02$. Multiplying b_r by a factor of 20 is the most effective treatment, bringing E_h above 90% into the healthy outcome category. Higher values of b_r increase E_h further. In this case, E_h does not respond to changes in k_{mne} or x_{mne}. Similarly to the previous case, the k_n intervention changes M1 dynamics the most but does not have a meaningful effect on healthy epithelial cells. Decreasing k_{en} has somewhat of an effect on E_h, in contrast to the case study shown in Figure 13 in which multiplying k_{en} by a factor greater than one increased E_h. Phagocytosis of damaged cells by neutrophils can make space for healthy epithelial cells to proliferate and fill the empty space, but neutrophils can also prevent these damaged cells from repairing on their own. We hypothesize that the latter is the reason for this inverse reaction from E_h.

A noticeable difference between the first case studied and the second two is M1 activation. In the first case, M1 macrophages reach almost 45% of total macrophages at the site of inflammation, whereas in the other two cases, there is barely any M1 activation at all. A successful intervention in the first case is paired with a lower peak in M1 and return to baseline. In the second case (Figure 15c), the only parameter that increases M1 levels above a negligible amount is k_n, but this does not translate to a change in outcome for E_h. The third case (Figure 15d) shows a variety of peaks depending on the intervention, but the y-axis reveals that the transients are below half a percent at their maximum. This points to the need for proper macrophage activation for epithelial health.

We are able to identify interventions that increase E_h back to a healthy state for two cases that start in a healthy state and end in persistent inflammation. Some treatments prove to be less effective in some scenarios and more effective in others. In the first and third cases, treatments change the steady-state so that the virtual patient stayed healthy after the intervention ended; in the second case, one intervention helped somewhat, but only lasted as long as the treatment period. One important distinction between all three cases is the variety in M1 activation. Furthermore, the case that responded the least to treatment is the one that started with persistent inflammation and ended in a dying disease progression. This may point to the idea that some cases are beyond intervention, or that further work on finding alternative

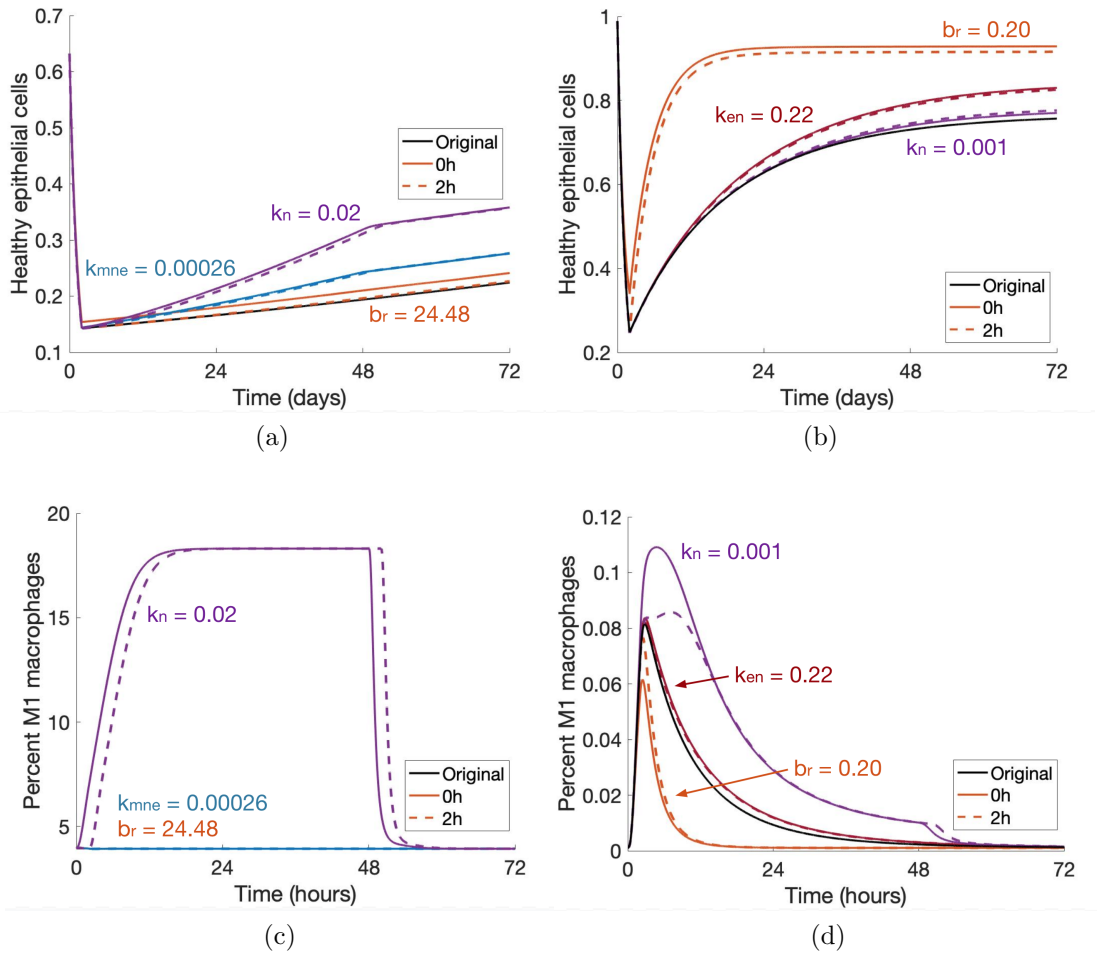

Figure 15: Possible intervention strategies for two additional case studies. (a, c): E_h and $M1$, respectively, for a case that begins in persistent inflammation and ends in a dying state. Original parameter values: $b_r = 1.22$, $k_{mne} = 0.005$, $x_{mne} = 2.71$ (not shown), $k_{en} = 2.31$ (not shown), and $k_n = 0.43$. (b, d): E_h and $M1$, respectively, for a case that begins healthy and ends in persistent inflammation. Original parameter values: $b_r = 0.010$, $k_{mne} = 0.015$ (not shown), $x_{mne} = 24.67$ (not shown), $k_{en} = 0.011$, and $k_n = 0.02$. Five different interventions to increase E_h are as follows: b_r multiplied by a factor of 20 (orange), k_{mne} multiplied by a factor of 0.05 (blue), x_{mne} multiplied by a factor of 0.05 (not shown), k_{en} multiplied by a factor of 0.05 (red), and k_n multiplied by a factor of 0.05 (purple). Interventions lasted for 48 hours, starting either at the beginning (0h) or end (2h) of ventilation.

interventions is needed.

4. Discussion

The spectrum of macrophage activation has been a recently growing field of research (Aggarwal et al., 2014; Mosser and Edwards, 2008; Torres et al., 2019). Mathematical models have studied a host of causes of lung inflammation including bacterial and viral infections and allergic reactions (Brown et al., 2011; Day et al., 2009; Manchanda et al., 2014; Smith et al., 2011). Models have also been studied to examine the effects of biomechanical strain on the lungs (Pidaparti et al., 2013). Our model combines the varied effects of macrophage activation with a more detailed epithelial subsystem. These features help to provide a better understanding of how the different macrophage phenotypes work together to bring about resolution after damage and how imbalances can cause a decline in health after ventilation.

We also examine how the recruitment of circulating immune cells from the bloodstream contributes to the immune response using a two-compartmental model. Our model incorporates a number of factors involved in the immune response, including naive M0, pro-inflammatory M1 and anti-inflammatory M2 macrophages, three states of epithelial cells (healthy, damaged, dead), activated and unactivated neutrophils, and various mediators used to signal between cells.

The model consists of 18 state equations and 67 parameters. Because of its large size, various methods were used to find biologically meaningful parameter sets that also made sense mathematically. Using Latin Hypercube Sampling, we found ranges of parameters that produced a variety of dynamics and used these ranges to produce 22,554 parameter sets. This "virtual cohort" reveals the variety of dynamics that can be generated by the model as well as the unique characteristics and properties of the transients that respond differently to treatments. We classified parameter sets into categories of healthy, persistent inflammation, and dying based on the percentage of healthy epithelial cells at the beginning or end of the simulation.

We then utilized several methods to determine the most important parameters for model output, particularly epithelial health. Using eFAST, a sensitivity analysis method for non-linear, non-monotonic ODEs, we found parameters that, when fluctuated, caused a statistically significant difference in output than that generated by a dummy parameter. We then compared these results with more non-conventional and less computationally intensive methods. The random forest decision tree algorithm was used to determine the importance of parameters and other predictors on epithelial health and is particularly useful for large data sets, such as the parameter sets in our virtual cohort. Additionally, significance testing was used to determine statistically significant differences in parameters grouped by outcome.

We were able to not only include parameter values but also other predictors later found to be important, including the M1 peak ratio and the difference between E_h initial condition and ending value. Three of the most important parameters were b_r, the rate of self-repair of epithelial cells, k_{mne}, the rate at which macrophages and neutrophils cause collateral damage to epithelial cells, x_{mne}, the Hill-type coefficient that regulates the effectiveness of that collateral damage, and k_{en}, the rate of phagocytosis of damaged epithelial cells by neutrophils. These important parameters and predictors were confirmed by at least two of the methods used.

Analysis showed that properties and parameters related to epithelial repair and M1 activation and de-activation were especially predictive of outcome. We used b_r, k_{mne}, x_{mne}, k_{en}, and k_n to simulate treatments for specific parameter sets in the virtual cohort that started in one disease progression state and ended in a lower one. Experimental data is limited for VILI, but we were able to use data from Misharin et al. (2013) as an initial starting point for biologically feasible dynamics. We found that modulating b_r is effective in most cases, and the other four can be helpful in some. Each of the three cases responded differently to treatment and these differences were paired with different M1 activation dynamics, indicating that macrophage activation is tied to epithelial health in VILI.

Further experimental data is necessary to better understand the dynamics of the immune response to VILI. The data available was a helpful starting point, but because of the experimental methods used, we were only able to use the data in terms of percentage of overall macrophages instead of concentrations. In the future, concentrations of macrophages and neutrophils, as well as a way to experimentally measure epithelial health at multiple time points would be extremely beneficial.

Another area of further study is determining why some virtual patients can recover with a short intervention while others need indefinite treatment. We hypothesize that this has to do with the initial conditions of the patient but more work should be done to obtain a definite answer. This would be helpful to better understand patients who undergo VILI since patients generally need ventilation because of a preexisting condition, and do not begin ventilation in a completely healthy state. In fact, this model could be extended to include other types of injury such as a bacterial or viral infection to study the interactions between the different types of injury and how they contribute to patient outcome.

In conclusion, our model contributes to the current understanding of macrophage activation in the context of lung inflammation, and is an especially important first step for VILI. Our parameter analysis using a variety of methods provides new insight into potential interventions during and after ventilation to mediate VILI. Additional experimental data will greatly improve our ability to suggest treatments. Further-

more, the model can be extended to include other types of injury that create the need for mechanical ventilation in the first place.

References

Aggarwal, N.R., King, L.S., D'Alessio, F.R., 2014. Diverse Macrophage Populations Mediate Acute Lung Inflammation and Resolution. American Journal of Physiology-Lung Cellular and Molecular Physiology 306, L709–L725. URL: http://www.physiology.org/doi/abs/10.1152/ajplung.00341.2013, doi:10.1152/ajplung.00341.2013.

Anderson, C.S., DeDiego, M.L., Topham, D.J., Thakar, J., 2016. Boolean Modeling of Cellular and Molecular Pathways Involved in Influenza Infection. Computational and Mathematical Methods in Medicine 2016. URL: https://www.ncbi.nlm.nih.gov/pmc/articles/PMC4769743/, doi:10.1155/2016/7686081.

Benjamini, Y., Hochberg, Y., 1995. Controlling the false discovery rate: a practical and powerful approach to multiple testing. Journal of the Royal statistical society: series B (Methodological) 57, 289–300.

Braun, D.A., Fribourg, M., Sealfon, S.C., 2013. Cytokine Response Is Determined by Duration of Receptor and Signal Transducers and Activators of Transcription 3 (STAT3) Activation. Journal of Biological Chemistry 288, 2986–2993. URL: http://www.jbc.org/content/288/5/2986, doi:10.1074/jbc.M112.386573.

Brown, B.N., Price, I.M., Toapanta, F.R., DeAlmeida, D.R., Wiley, C.A., Ross, T.M., Oury, T.D., Vodovotz, Y., 2011. An Agent-Based Model of Inflammation and Fibrosis Following Particulate Exposure in the Lung. Mathematical Biosciences 231, 186–196. URL: http://www.sciencedirect.com/science/article/pii/S0025556411000356, doi:10.1016/j.mbs.2011.03.005.

Brown, D., Namas, R.A., Almahmoud, K., Zaaqoq, A., Sarkar, J., Barclay, D.A., Yin, J., Ghuma, A., Abboud, A., Constantine, G., Nieman, G., Zamora, R., Chang, S.C., Billiar, T.R., Vodovotz, Y., 2015. Trauma in silico: Individual-specific mathematical models and virtual clinical populations. Science Translational Medicine 7, 285ra61–285ra61. URL: https://stm.sciencemag.org/content/7/285/285ra61, doi:10.1126/scitranslmed.aaa3636.

Bruno, G., Perelli, S., Fabrizio, C., Buccoliero, G.B., 2020. Short-term outcomes in individuals aged 75 or older with severe coronavirus disease (COVID-19): First observations from an Infectious Diseases Unit in Southern Italy. The Journal of Infection URL: https://www.ncbi.nlm.nih.gov/pmc/articles/PMC7224683/, doi:10.1016/j.jinf.2020.05.024.

Canan, C.H., Gokhale, N.S., Carruthers, B., Lafuse, W.P., Schlesinger, L.S., Torrelles, J.B., Turner, J., 2014. Characterization of Lung Inflammation and its Impact on Macrophage Function in Aging. Journal of Leukocyte Biology 96, 473–480. URL: http://www.jleukbio.org.proxy.library.vcu.edu/content/96/3/473, doi:10.1189/jlb.4A0214-093RR.

Chernyavsky, I.L., Croisier, H., Chapman, L.A.C., Kimpton, L.S., Hiorns, J.E., Brook, B.S., Jensen, O.E., Billington, C.K., Hall, I.P., Johnson, S.R., 2014. The Role of Inflammation Resolution Speed in Airway Smooth Muscle Mass Accumulation in Asthma: Insight from a Theoretical Model. PLOS ONE 9, e90162. URL: http://journals.plos.org/plosone/article?id=10.1371/journal.pone.0090162, doi:10.1371/journal.pone.0090162.

Collins, D.C., Avissar, R., 1994. An Evaluation with the Fourier Amplitude Sensitivity Test (FAST) of Which Land-Surface Parameters Are of Greatest Importance in Atmospheric Modeling. Journal of Climate 7, 681–703.

Crosby, L.M., Waters, C.M., 2010. Epithelial Repair Mechanisms in the Lung. American Journal of Physiology-Lung Cellular and Molecular Physiology 298, L715–L731. URL: http://www.physiology.org/doi/abs/10.1152/ajplung.00361.2009, doi:10.1152/ajplung.00361.2009.

Cukier, R.I., Fortuin, C.M., Shuler, K.E., Petschek, A.G., Schaibly, J.H., 1973. Study of the sensitivity of coupled reaction systems to uncertainties in rate coefficients. I Theory. The Journal of Chemical Physics 59, 3873–3878. URL: https://aip.scitation.org/doi/abs/10.1063/1.1680571, doi:10.1063/1.1680571.

Day, J., Friedman, A., Schlesinger, L.S., 2009. Modeling the Immune Rheostat of Macrophages in the Lung in Response to Infection. Proceedings of the National Academy of Sciences 106, 11246–11251. URL: http://www.pnas.org.proxy.library.vcu.edu/content/106/27/11246, doi:10.1073/pnas.0904846106.

De Rekeneire, N., Peila, R., Ding, J., Colbert, L.H., Visser, M., Shorr, R.I., Kritchevsky, S.B., Kuller, L.H., Strotmeyer, E.S., Schwartz, A.V., et al., 2006. Diabetes, hyperglycemia, and inflammation in older individuals: the health, aging and body composition study. Diabetes care 29, 1902–1908.

Feng, Y., Amoateng-Adjepong, Y., Kaufman, D., Gheorghe, C., Manthous, C.A., 2009. Age, duration of mechanical ventilation, and outcomes of patients who are critically ill. Chest 136, 759–764.

Gardner, A., Borthwick, L.A., Fisher, A.J., 2010. Lung Epithelial Wound Healing in Health and Disease. Expert Review of Respiratory Medicine 4, 647–660. URL: https://doi.org/10.1586/ers.10.62, doi:10.1586/ers.10.62.

Golov, A., Simakov, S., Soe, Y.N., Pryamonosov, R., Mynbaev, O., Kholodov, A., 2017. Multiscale CT-Based Computational Modeling of Alveolar Gas Exchange during Artificial Lung Ventilation, Cluster (Biot) and Periodic (Cheyne-Stokes) Breathings and Bronchial Asthma Attack. Computation 5, 11. URL: http://www.mdpi.com/2079-3197/5/1/11, doi:10.3390/computation5010011.

Gordon, S., 2003. Alternative Activation of Macrophages. Nature Reviews Immunology 3, 23–35. URL: http://www.nature.com/articles/nri978, doi:10.1038/nri978.

Grommes, J., Soehnlein, O., 2011. Contribution of Neutrophils to Acute Lung Injury. Molecular Medicine 17, 293–307. URL: https://www.ncbi.nlm.nih.gov/pmc/articles/PMC3060975/, doi:10.2119/molmed.2010.00138.

Halbertsma, F.J.J., Vaneker, M., Scheffer, G.J., van der Hoeven, J.G., 2005. Cytokines and biotrauma in ventilator-induced lung injury: a critical review of the literature. The Netherlands Journal of Medicine 63, 382–392.

Hancioglu, B., Swigon, D., Clermont, G., 2007. A Dynamical Model of Human Immune Response to Influenza A Virus Infection. Journal of Theoretical Biology 246, 70–86. URL: http://www.sciencedirect.com/science/article/pii/S0022519306005820, doi:10.1016/j.jtbi.2006.12.015.

Herbert, J.A., Valentine, M.S., Saravanan, N., Schneck, M.B., Pidaparti, R., Fowler III, A.A., Reynolds, A.M., Heise, R.L., 2016. Conservative fluid management prevents age-associated ventilator induced mortality. Experimental gerontology 81, 101–109.

Herold, S., Mayer, K., Lohmeyer, J., 2011. Acute Lung Injury: How Macrophages Orchestrate Resolution of Inflammation and Tissue Repair. Frontiers in Immunology 2. URL: https://www.ncbi.nlm.nih.gov/pmc/articles/PMC3342347/, doi:10.3389/fimmu.2011.00065.

Heusinkveld, M., Steenwijk, P.J.d.V.v., Goedemans, R., Ramwadhdoebe, T.H., Gorter, A., Welters, M.J.P., Hall, T.v., Burg, S.H.v.d., 2011. M2 Macrophages Induced by Prostaglandin E2 and IL-6 from Cervical Carcinoma Are Switched to Activated M1 Macrophages by CD4+ Th1 Cells. The Journal of Immunology 187, 1157–1165. URL: http://www.jimmunol.org/content/187/3/1157, doi:10.4049/jimmunol.1100889.

Hickling, K.G., 1998. The Pressure–Volume Curve Is Greatly Modified by Recruitment. American Journal of Respiratory and Critical Care Medicine 158, 194–202. doi:10.1164/ajrccm.158.1.9708049.

Johnston, L.K., Rims, C.R., Gill, S.E., McGuire, J.K., Manicone, A.M., 2012. Pulmonary Macrophage Subpopulations in the Induction and Resolution of Acute Lung Injury. American Journal of Respiratory Cell and Molecular Biology URL: http://www.atsjournals.org/doi/abs/10.1165/rcmb.2012-0090OC, doi:10.1165/rcmb.2012-0090OC.

Kirschner, D.E., 2008. Matlab Functions for PRCC and eFAST. URL: http://malthus.micro.med.umich.edu/lab/usadata/.

Kolaczkowska, E., Kubes, P., 2013. Neutrophil Recruitment and Function in Health and Inflammation. Nature Reviews Immunology 13, 159–175. URL: https://www.nature.com/articles/nri3399, doi:10.1038/nri3399.

Kumar, V., Sharma, A., 2010. Neutrophils: Cinderella of Innate Immune System. International Immunopharmacology 10, 1325–1334. URL: http://www.sciencedirect.com/science/article/pii/S1567576910002663, doi:10.1016/j.intimp.2010.08.012.

Le, J., 2018. Decision Trees in R. URL: https://www.datacamp.com/community/tutorials/decision-trees-R.

Liaw, A., Wiener, M., 2002. Classification and Regression by randomForest 2, 6.

Linehan, E., Fitzgerald, D., 2015. Ageing and the Immune System: Focus on Macrophages. European Journal of Microbiology and Immunology

5, 14–24. URL: http://akademiai.com/doi/abs/10.1556/EuJMI-D-14-00035, doi:10.1556/EuJMI-D-14-00035.

Mahase, E., 2020. Covid-19: most patients require mechanical ventilation in first 24 hours of critical care. BMJ 368. URL: https://www.bmj.com/content/368/bmj.m1201, doi:10.1136/bmj.m1201. publisher: British Medical Journal Publishing Group Section: News.

Mahbub, S., Deburghgraeve, C.R., Kovacs, E.J., 2011. Advanced Age Impairs Macrophage Polarization. Journal of Interferon & Cytokine Research 32, 18–26. URL: http://online.liebertpub.com/doi/abs/10.1089/jir.2011.0058, doi:10.1089/jir.2011.0058.

Maiti, S., Dai, W., Alaniz, R.C., Hahn, J., Jayaraman, A., 2014. Mathematical Modeling of Pro- and Anti-Inflammatory Signaling in Macrophages. Processes 3, 1–18. URL: http://www.mdpi.com/2227-9717/3/1/1, doi:10.3390/pr3010001.

Manchanda, H., Seidel, N., Krumbholz, A., Sauerbrei, A., Schmidtke, M., Guthke, R., 2014. Within-Host Influenza Dynamics: A Small-Scale Mathematical Modeling Approach. Biosystems 118, 51–59. URL: http://www.sciencedirect.com/science/article/pii/S0303264714000331, doi:10.1016/j.biosystems.2014.02.004.

Marini, J.J., Crooke, P.S., Truwit, J.D., 1989. Determinants and Limits of Pressure-Preset Ventilation: a Mathematical Model of Pressure Control. Journal of Applied Physiology 67, 1081–1092. URL: http://jap.physiology.org.proxy.library.vcu.edu/content/67/3/1081.

Marino, S., Hogue, I.B., Ray, C.J., Kirschner, D.E., 2008. A methodology for performing global uncertainty and sensitivity analysis in systems biology. Journal of Theoretical Biology 254, 178–196. URL: http://www.sciencedirect.com/science/article/pii/S0022519308001896, doi:10.1016/j.jtbi.2008.04.011.

Mason, R.J., 2006. Biology of alveolar type II cells. Respirology 11, S12–S15. URL: https://onlinelibrary.wiley.com/doi/abs/10.1111/j.1440-1843.2006.00800.x, doi:10.1111/j.1440-1843.2006.00800.x.

Matthay, M.A., Robriquet, L., Fang, X., 2005. Alveolar Epithelium. Proceedings of the American Thoracic Society 2, 206–213. URL:

https://www.atsjournals.org/doi/full/10.1513/pats.200501-009AC, doi:10.1513/pats.200501-009AC.

McKay, M.D., Beckman, R.J., Conover, W.J., 1979. Comparison of Three Methods for Selecting Values of Input Variables in the Analysis of Output from a Computer Code. Technometrics 21, 239–245. doi:10.1080/00401706.1979.10489755.

McKight, P.E., Najab, J., 2010. Kruskal-Wallis Test, in: The Corsini Encyclopedia of Psychology. American Cancer Society, pp. 1–1. URL: https://onlinelibrary.wiley.com/doi/abs/10.1002/9780470479216.corpsy0491, doi:10.1002/9780470479216.corpsy0491.

Misharin, A.V., Morales-Nebreda, L., Mutlu, G.M., Budinger, G.R.S., Perlman, H., 2013. Flow Cytometric Analysis of Macrophages and Dendritic Cell Subsets in the Mouse Lung. American Journal of Respiratory Cell and Molecular Biology 49, 503–510. URL: https://www.ncbi.nlm.nih.gov/pmc/articles/PMC3824047/, doi:10.1165/rcmb.2013-0086MA.

Mochan, E., Swigon, D., Ermentrout, G.B., Lukens, S., Clermont, G., 2014. A Mathematical Model of Intrahost Pneumococcal Pneumonia Infection Dynamics in Murine Strains. Journal of Theoretical Biology 353, 44–54. URL: http://www.sciencedirect.com/science/article/pii/S0022519314000964, doi:10.1016/j.jtbi.2014.02.021.

Mosser, D.M., Edwards, J.P., 2008. Exploring the Full Spectrum of Macrophage Activation. Nature Reviews Immunology 8, 958–969. URL: http://www.nature.com.proxy.library.vcu.edu/nri/journal/v8/n12/full/nri2448.html, doi:10.1038/nri2448.

Nathan, C., 2006. Neutrophils and Immunity: Challenges and Opportunities. Nature Reviews Immunology 6, 173–182. URL: https://www.nature.com/articles/nri1785, doi:10.1038/nri1785.

Naylor, E.J., Bakstad, D., Biffen, M., Thong, B., Calverley, P., Scott, S., Hart, C.A., Moots, R.J., Edwards, S.W., 2007. Haemophilus Influenzae Induces Neutrophil Necrosis. American Journal of Respiratory Cell and Molecular Biology 37, 135–143. URL: https://www.atsjournals.org/doi/full/10.1165/rcmb.2006-0375OC, doi:10.1165/rcmb.2006-0375OC.

Opal, S.M., DePalo, V.A., 2000. Anti-inflammatory cytokines. Chest 117, 1162–1172.

Pidaparti, R.M., Burnette, M., Heise, R.L., Reynolds, A., 2013. Analysis for Stress Environment in the Alveolar Sac Model. Journal of biomedical science and engineering 6, 901–907. URL: http://www.ncbi.nlm.nih.gov/pmc/articles/PMC4057278/, doi:10.4236/jbise.2013.69110.

Pothen, J.J., Poynter, M.E., Bates, J.H.T., 2015. A Computational Model of Unresolved Allergic Inflammation in Chronic Asthma. American Journal of Physiology - Lung Cellular and Molecular Physiology 308, L384–L390. URL: http://ajplung.physiology.org.proxy.library.vcu.edu/content/308/4/L384, doi:10.1152/ajplung.00268.2014.

Provinciali, M., Cardelli, M., Marchegiani, F., 2011. Inflammation, chronic obstructive pulmonary disease and aging. Current Opinion in Pulmonary Medicine 17, S3. doi:10.1097/01.mcp.0000410742.90463.1f.

Raman, K., Bhat, A.G., Chandra, N., 2010. A Systems Perspective of Host–Pathogen Interactions: Predicting Disease Outcome in Tuberculosis. Molecular BioSystems 6, 516–530. URL: http://pubs.rsc.org/en/content/articlelanding/2010/mb/b912129c, doi:10.1039/B912129C.

Reynolds, A., Bard Ermentrout, G., Clermont, G., 2010. A Mathematical Model of Pulmonary Gas Exchange Under Inflammatory Stress. Journal of Theoretical Biology 264, 161–173. URL: http://www.sciencedirect.com/science/article/pii/S0022519310000159, doi:10.1016/j.jtbi.2010.01.011.

Robb, C.T., Regan, K.H., Dorward, D.A., Rossi, A.G., 2016. Key Mechanisms Governing Resolution of Lung Inflammation. Seminars in Immunopathology 38, 425–448. URL: https://link-springer-com.proxy.library.vcu.edu/article/10.1007/s00281-016-0560-6, doi:10.1007/s00281-016-0560-6.

Saltelli, A., Bolado, R., 1998. An alternative way to compute Fourier amplitude sensitivity test (FAST). Computational Statistics & Data Analysis 26, 445–460. URL: http://www.sciencedirect.com/science/article/pii/S0167947397000431, doi:10.1016/S0167-9473(97)00043-1.

Saltelli, A., Tarantola, S., Campolongo, F., Ratto, M., 2004. Sensitivity Analysis in Practice: A Guide to Assessing Scientific Models. John Wiley & Sons. Google-Books-ID: NsAVmohPNpQC.

Saltelli, A., Tarantola, S., Chan, K.P.S., 1999. A Quantitative Model-Independent Method for Global Sensitivity Analysis of Model Output. Technometrics 41, 39–56. URL: https://www.tandfonline.com/doi/abs/10.1080/00401706.1999.10485594, doi:10.1080/00401706.1999.10485594.

Schaibly, J.H., Shuler, K.E., 1973. Study of the sensitivity of coupled reaction systems to uncertainties in rate coefficients. II Applications. The Journal of Chemical Physics 59, 3879–3888. URL: https://aip.scitation.org/doi/abs/10.1063/1.1680572, doi:10.1063/1.1680572.

Schirm, S., Ahnert, P., Wienhold, S., Mueller-Redetzky, H., Nouailles-Kursar, G., Loeffler, M., Witzenrath, M., Scholz, M., 2016. A Biomathematical Model of Pneumococcal Lung Infection and Antibiotic Treatment in Mice. PLOS ONE 11, e0156047. URL: http://journals.plos.org/plosone/article?id=10.1371/journal.pone.0156047, doi:10.1371/journal.pone.0156047.

Segovia-Juarez, J.L., Ganguli, S., Kirschner, D., 2004. Identifying Control Mechanisms of Granuloma Formation During M. tuberculosis Infection Using an Agent-Based Model. Journal of Theoretical Biology 231, 357–376. URL: http://www.sciencedirect.com/science/article/pii/S0022519304003212, doi:10.1016/j.jtbi.2004.06.031.

Slutsky, A.S., Ranieri, V.M., 2013. Ventilator-Induced Lung Injury. New England Journal of Medicine 369, 2126–2136. URL: http://dx.doi.org/10.1056/NEJMra1208707, doi:10.1056/NEJMra1208707.

Smith, A.M., McCullers, J.A., Adler, F.R., 2011. Mathematical Model of a Three-Stage Innate Immune Response to a Pneumococcal Lung Infection. Journal of Theoretical Biology 276, 106–116. URL: http://www.sciencedirect.com/science/article/pii/S0022519311000786, doi:10.1016/j.jtbi.2011.01.052.

Soehnlein, O., Lindbom, L., 2010. Phagocyte partnership during the onset and resolution of inflammation. Nature Reviews Immunology 10, 427–439. URL: https://www.nature.com/articles/nri2779, doi:10.1038/nri2779.

Summers, C., Rankin, S.M., Condliffe, A.M., Singh, N., Peters, A.M., Chilvers, E.R., 2010. Neutrophil Kinetics in Health and Disease. Trends in Immunology 31, 318–324. URL: http://www.sciencedirect.com/science/article/pii/S147149061000075X, doi:10.1016/j.it.2010.05.006.

Torres, M., Wang, J., Yannie, P.J., Ghosh, S., Segal, R.A., Reynolds, A.M., 2019. Identifying important parameters in the inflammatory process with a mathematical model of immune cell influx and macrophage polarization. PLOS Computational Biology 15, e1007172. URL: https://journals.plos.org/ploscompbiol/article?id=10.1371/journal.pcbi.1007172, doi:10.1371/journal.pcbi.1007172.

Vlahakis, N.E., Schroeder, M.A., Limper, A.H., Hubmayr, R.D., 1999. Stretch Induces Cytokine Release by Alveolar Epithelial Cells in Vitro. American Journal of Physiology-Lung Cellular and Molecular Physiology 277, L167–L173. URL: http://www.physiology.org/doi/abs/10.1152/ajplung.1999.277.1.L167, doi:10.1152/ajplung.1999.277.1.L167.

Wang, N., Liang, H., Zen, K., 2014. Molecular Mechanisms That Influence the Macrophage M1–M2 Polarization Balance. Frontiers in Immunology 5. URL: http://www.ncbi.nlm.nih.gov/pmc/articles/PMC4246889/, doi:10.3389/fimmu.2014.00614.

Ware, L.B., Matthay, M.A., 2000. The Acute Respiratory Distress Syndrome. New England Journal of Medicine 342, 1334–1349. URL: https://doi.org/10.1056/NEJM200005043421806, doi:10.1056/NEJM200005043421806.

Wu, Z., McGoogan, J.M., 2020. Characteristics of and Important Lessons From the Coronavirus Disease 2019 (COVID-19) Outbreak in China: Summary of a Report of 72 314 Cases From the Chinese Center for Disease Control and Prevention. JAMA 323, 1239–1242. URL: https://jamanetwork.com/journals/jama/fullarticle/2762130, doi:10.1001/jama.2020.2648. publisher: American Medical Association.

Yu, Y.R.A., Hotten, D.F., Malakhau, Y., Volker, E., Ghio, A.J., Noble, P.W., Kraft, M., Hollingsworth, J.W., Gunn, M.D., Tighe, R.M., 2016. Flow cytometric analysis of myeloid cells in human blood, bronchoalveolar lavage, and lung tissues. American journal of respiratory cell and molecular biology 54, 13–24.